

2011

Recurrent voluminous sector collapses at Volcán Barú, Panama

Julie A. Herrick
Michigan Technological University

Follow this and additional works at: <https://digitalcommons.mtu.edu/etds>



Part of the [Geology Commons](#)

Copyright 2011 Julie A. Herrick

Recommended Citation

Herrick, Julie A., "Recurrent voluminous sector collapses at Volcán Barú, Panama", Master's Thesis, Michigan Technological University, 2011.
<https://doi.org/10.37099/mtu.dc.etds/324>

Follow this and additional works at: <https://digitalcommons.mtu.edu/etds>



Part of the [Geology Commons](#)

Recurrent voluminous sector collapses at Volcán Barú, Panama

Julie A. Herrick

A THESIS

Submitted in partial fulfillment of the requirements

for the degree of

MASTER OF SCIENCE IN GEOLOGY

MICHIGAN TECHNOLOGICAL UNIVERSITY

2011

Copyright © Julie A. Herrick 2011

This thesis, "Recurrent voluminous sector collapses at Volcán Barú, Panama,"
is hereby approved in partial fulfillment of the requirements for the Degree of
MASTER OF SCIENCE IN GEOLOGY.

Department:

Geological and Mining Engineering and Sciences

Signatures:

Thesis Advisor _____
Dr. William I. Rose

Department Chair _____
Dr. Wayne Pennington

Date _____

Abstract

Two volcanic debris avalanche deposits (VDADs), both attributed to sector collapse at Volcán Barú, Panama, have been identified after an investigation of deposits that covered more than a thousand square kilometers. The younger Barriles Deposit is constrained by two radiocarbon ages that are ~9 ka; the older Caisán Deposit is at or beyond the radiocarbon range, >43,500 ybp. The total runout length of the Caisán Deposit was ~50 km and it covers 1190 km². The Barriles Deposit extended to about 45 km and covered an area of 966 km², overlapping most of the Caisán. The VDADs are blanketed by pyroclastic deposits and contain a predominance of andesitic material likely representing volcanic dome rock which accumulated above the active vent at Barú before collapsing. Despite heavy vegetation in the field area, over 4000 individual hummocks were digitized from aerial photography. Statistical analysis of hummock locations and geometries depict flow patterns of highly- fragmented material reflecting the effects of underlying topography and also help to define the limit of Barriles' shorter termination.

Barriles and Caisán are primarily unconfined, subaerial volcanic deposits that are among the world's most voluminous. Calculated through two different geospatial processes, thickness values from field measurements and inferences yield volumes >30 km³ for both deposits. VDADs of comparable scale come from Mount Shasta, USA; Socompa, Chile/Argentina; and Shiveluch, Russia. Currently, the modern edifice is 200-400m lower than the pre-collapse Barriles and Caisán summits and only 16-25% of the former edifice has been replaced since the last failure.

Acknowledgements

Financial support for this work came from the US National Science Foundation (PIRE 0530109) which paid for course credits at Michigan Tech, field costs for several visitors to my field area, maps, aerial photographs and fieldwork costs. The US Geological Survey paid for the radiocarbon determinations of charcoal specimens through James Vallance and David Sherrod. The US Peace Corps established my two-year volunteership in western Panama and provided in-country support for field research and just as important, secured aqueduct project success in Quebrada Mina.

Primary thanks go to my advisor and committee: William I. Rose, Blair Orr, and Lee Siebert. To Peace Corps Panama colleagues: Timothy Wellman, Carlos Moreno, and Lourdes Rodriguez. For their hospitality, generosity, and inspiration, I'm indebted to the communities of Calabazal and Quebrada Mina in the Comarca Ngäbe-Buglé and my counterparts (o en otras palabras: mi equipo): Román and Eliecer Rodriguez Chávez and Miguel Pedrol Mora. To the MTU community: Rüdiger Escobar Wolf for the Matlab and GIS advice and general philosophical embiggening; Miriam Rios Sanchez; Elisabet Head; compatriot RCPVs: Luke Bowman, Kyle Brill, Lindsey Brown, Jemile Erdem, Randal Fish, Emily Gochis, Matt Kucharski, Hans Lechner, John Lyons, Jarod Maggio, Essa Paterson, Cara Shonsey, Jesse Silverman, Gwynneth Smith, Robert Hegemann, Lara Kapelanczyk – for their support, compassion, and encouragement to the utmost.

For developing the ingenious MatLab script for pulling measurements from shapefiles, my sincere thanks to Ruben Otoniel Matias Gomez (and extra thanks to Rüdiger for helping me to customize it for the biggest avalanche in the world!). For the feedback and support State-side: Karen Holmberg, Kristin Morell, and Benjamin van Wyk DeVries. For the Panama-side support: the Sinaproc staff: Director José Donderis, José A. Guerra, and Ana Isabel Gómez Araúz; the IGNTG staff: Luis Armuelles and Director

José de la Luz in Photogrammetry, Primola and Myra in Mapoteca; Carla Black & Ángel Rodríguez in Volcán for both the hospitality and brainstorming sessions; Kevin Mellinger the rafting guy; Guillermo Alvarado for field guidance; and University of Panama scientists: Director Eduardo Comacho, Arkin Tapia, and Eric Chichaco.

I am grateful for the quality control and technical advice from Steve Schilling (CVO), and Frank Trusdell (HVO). David Sherrod and James Vallance (CVO) generously supported the radiocarbon analysis while also sharing data and field experience.

For the valuable discussions and sharing debris avalanche data from Parinacota, Chile and Mombacho, Nicaragua, Thomas Shea deserves “one big mahalo.”

For inspiration, mentoring, and promoting my enthusiasm for boots-on-the-ground fieldwork: Frank Trusdell, Jack Lockwood, Todd & Jenn Cullings, Mel Essington, John Brady, Julia Baldwin, Erika Ronchin, Jessica Wardlaw, Darwina Griffin, Sarah Henton, and Saskia van Manen.

Contents

ABSTRACT	III
ACKNOWLEDGEMENTS	IV
CONTENTS.....	VI
FIGURES	VIII
TABLES	X
INTRODUCTION	2
GEOLOGIC SETTING	2
RECENT ACTIVITY	3
TERMINOLOGY	5
METHODS	8
FIELDWORK	8
HUMMOCKS: DIGITIZING.....	10
DEBRIS AVALANCHE DEPOSITS.....	12
BARRILES DEPOSIT (VDADII)	13
CAISÁN DEPOSIT (VDADI).....	16
SEDIMENTARY ARCHITECTURE	22
SUMMARY OF FIELD CHARACTERISTICS	23
RADIOCARBON DATING	26
HUMMOCK GEOMETRY AND DISTRIBUTION	27
HUMMOCK PROXIMITY	31
VOLUME CALCULATION: DEPOSIT THICKNESSES.....	34
VOLUME CALCULATIONS: EDIFICE RECONSTRUCTION	38
DISCUSSION	44
SOURCES AND TIMING OF EVENTS.....	44
HUMMOCK DATA COMPARISONS	48
VDAD MOBILITY	50
CONCLUSIONS	53

REFERENCES	55
APPENDIX	61
LOCATION MAP	61
DEPOSIT MINERALOGY	62
REGIONAL GEOLOGY	63
RADIOCARBON PLOTS	65
MAP OF HUMMOCK ORIENTATIONS	66
MAPS OF DEPOSITS AND HUMMOCKS	67

Figures

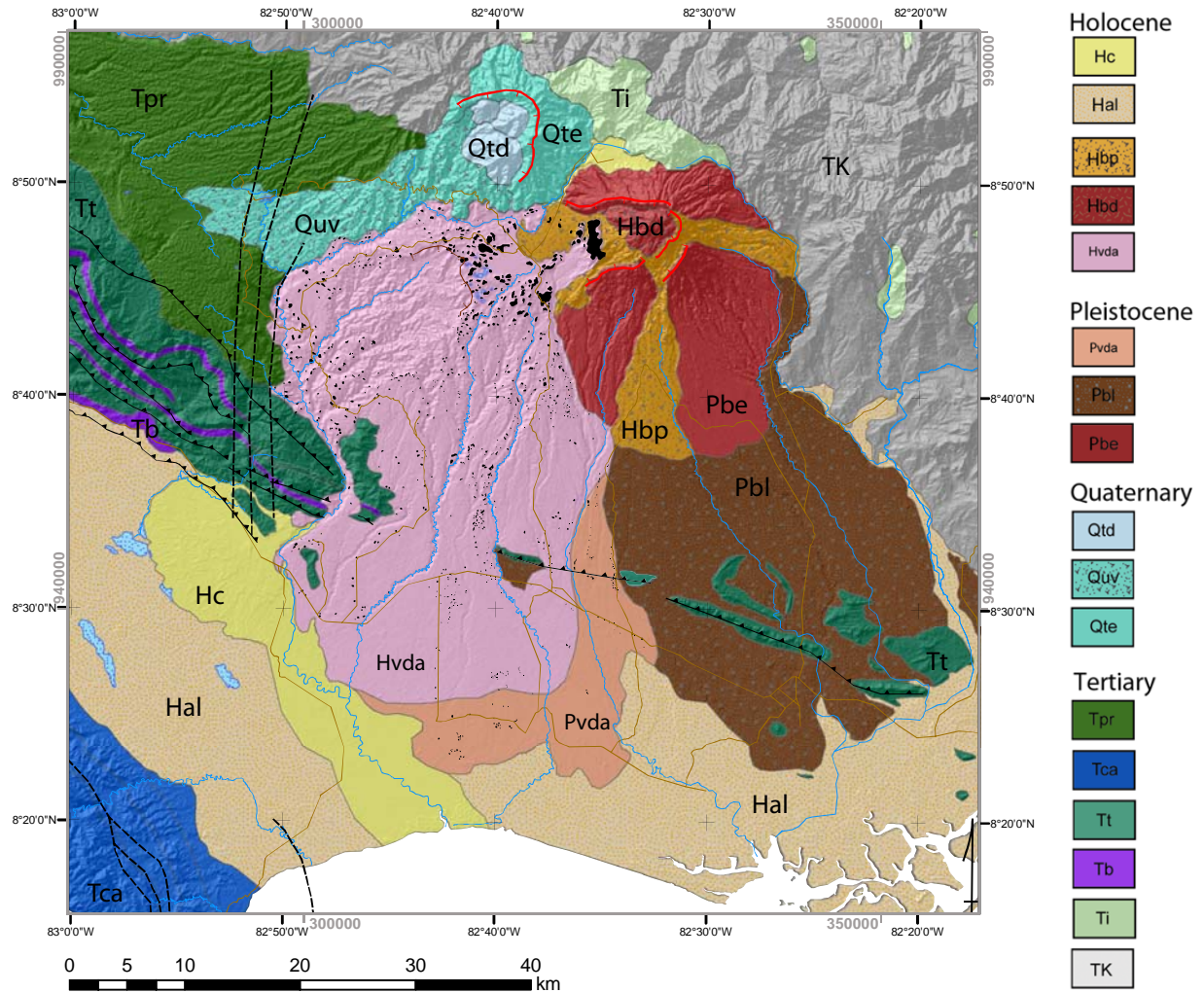
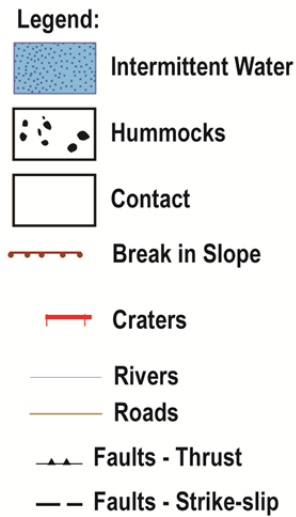
FIGURE 1 REGIONAL GEOLOGIC MAP OF WESTERN CHIRIQUÍ PROVINCE, PANAMA	1
FIGURE 2 MAP OF AREAL EXTENT OF DEBRIS AVALANCHES RECOGNIZED IN THIS STUDY.....	9
FIGURE 3 HUMMOCK EXAMPLE.....	10
FIGURE 4 PHOTO CROSS-SECTION SHOWING THE TWO VDADS SEPARATED BY SEDIMENTARY UNITS.....	12
FIGURE 5 BARRILES DEPOSIT: BLOCK FACIES	15
FIGURE 6 BARRILES DEPOSIT: MIXED FACIES	16
FIGURE 7 CAISÁN DEPOSIT: BLOCK FACIES.....	17
FIGURE 8 CAISÁN DEPOSIT: MIXED FACIES	19
FIGURE 9 CAISÁN DEPOSIT: A CLASTIC DIKE.....	20
FIGURE 10 UPPER CONTACT OF THE CAISÁN DEPOSIT	22
FIGURE 11 UPPER CONTACT OF THE BARRILES DEPOSIT	23
FIGURE 12 CHARRED WOOD WITHIN THE BARRILES DEPOSIT.....	25
FIGURE 13 EXAMPLES OF POLYGON GEOMETRIES.....	28
FIGURE 14 PLOT OF HUMMOCK AREA/DISTANCE.....	30
FIGURE 15 MAP OF AERIAL COVERAGE AND DIGITIZED HUMMOCKS.....	33
FIGURE 16 THICKNESS POLYGONS OF BARRILES AND CAISÁN DEPOSITS ..	37
FIGURE 17 DEM OF BARRILES AND CAISÁN DEPOSIT VOLUMES	38
FIGURE 18 10M DEM OF VOLCÁN BARÚ REGION AND SLOPE MAP.	39
FIGURE 19 ISOLATED EDIFICE LIMITS	40
FIGURE 20 3D VIEW OF BARÚ'S CURRENT EDIFICE.	40
FIGURE 21 3D VIEW OF BARÚ: BARRILES MODEL	41
FIGURE 22 PLAN VIEW OF BARÚ: BARRILES MODEL	42
FIGURE 23 SITES FOR RADIOMETRIC SAMPLES.....	46
FIGURE 24 PLOT OF 10 LARGEST HUMMOCK DIAMETERS (DIAM/DIST)	48
FIGURE 25 PLOT OF HUMMOCK DIAMETER/DISTANCE: VOLCÁN BARÚ: BARRILES AND CAISÁN, PARINACOTA, MOMBACHO: EL CRATER AND LAS ISLETAS, MOUNT SHASTA, AND MOUNT ST. HELENS	49
FIGURE 26 PLOT OF HEIGHT/LENGTH OF 40 VDADS	52

FIGURE 27 PLOT OF DEPOSIT AREA/VOLUME FROM 40 VDADS.	53
FIGURE 28 LOCATION MAP OF PANAMA AND STUDY AREA	61
FIGURE 29 GEOLOGIC DESCRIPTIONS FOR UNITS	63
FIGURE 30 RADIOCARBON PLOTS: BARRILES AND CAISÁN SAMPLES	65
FIGURE 31 MAP OF HUMMOCK ORIENTATIONS	66
FIGURE 32 EXAMPLES OF VDADS FROM FIVE VOLCANOES LOCATED IN DIFFERENT COUNTRIES.....	67

Tables

TABLE 1 PRINCIPAL RESOURCES FOR REGIONAL GEOLOGIC DATA	2
TABLE 2 TIMING OF HOLOCENE VOLCANIC ACTIVITY	4
TABLE 3 CLAST AND BLOCK SIZE VALUES.....	21
TABLE 4 RADIOCARBON AGES FROM VOLCÁN BARÚ'S VDADS	27
TABLE 5 HUMMOCK STATISTICS ZONES 1-6.....	29
TABLE 6 HUMMOCK PROXIMITY VALUES	31
TABLE 7 (NEXT PAGE) THICKNESS POINTS.	35
TABLE 8 VOLUME ESTIMATES OF VOLCÁN BARÚ'S VDADS.....	43
TABLE 9 RADIOMETRIC DATES FROM BARÚ REGION	45
TABLE 10 EXAMPLES OF SUBAERIAL VDADS.	50
TABLE 11 DEPOSIT MINERALOGY OF SAMPLES: BARRILES AND CAISÁN DEPOSITS	62

Figure 1 Regional geologic map of western Chiriquí Province, Panama. Compiled from sources listed in Table 1. Detailed descriptions of the geological units appear in the Appendix, Figure 33 “Regional Geology.”



Introduction

Geologic Setting

Southwestern Panama is tectonically active (Benjamín, 2004; Camacho and Benito, 2008; Mann et al., 2007) and two Pleistocene volcanic centers dominate the landscape of the Chiriquí Province (Figure 1). South of Panama's continental divide, volcanic deposits can be traced to Tisingal (also named Cerro Colorado) and Volcán Barú. While Tisingal is believed to be extinct, evidence of recent activity at Volcán Barú includes the recent volcanic deposits that blanket the Boquete and Horqueta Districts (Restrepo, 1987; Sherrod et al., 2007; UTP, 1992). While a major horseshoe-shaped crater breaches a sector of 10x6 km, the geomorphology of Barú reflects minimal flank erosion. The regional geologic map (Figure 1) synthesizes fieldwork and data from various investigators (Table 1).

The geologically recent volcanism at Volcán Barú suggests this area is the southern reach of the Central American Volcanic Arc (Siebert et al., 2006).

TABLE 1 PRINCIPAL RESOURCES FOR THE REGIONAL GEOLOGIC DATA IN FIGURE 1

	Geologic Region	References
1	Punta Burica Region	(Buchs et al., 2009) (Coates et al., 1992)
2	Fila Costeña Thrust Belt	(Morell et al., 2008) (de Boer et al., 1995)
3	Tisingal Volcanic Edifice and Dome Complex	(UTP, 1992) (Restrepo, 1987) (IRHE, 1984) (Stewart, 1978)
4	Volcán Barú Edifice and Dome Complex	(UTP, 1992) (Restrepo, 1987) (IRHE, 1984) (Stewart, 1978) (Sherrod et al., 2007)
5	Volcán Barú Debris Avalanche Deposits	(Sherrod et al., 2007) (Stewart, 1978)
6	Panama's regional geology	(Buchs et al., 2009) (French and Schenk, 2004) (Stewart, 1978) (Minerales, 1976, 1991)

Diminished volcanic activity and larger gaps between Panama's volcanoes correlates with the presence of the Nazca Plate and high-angle subduction (de Boer et al., 1995). The region is a transition along the Ring of Fire as it continues along the Pacific Rim to the South American Volcanic Arc. Carr et al. (2003; 2007) and Wegner et al. (2011) agree that the Panama Block is a region of transition and terminate the Central American chain in Costa Rica, west of Volcán Barú and Tisingal. Along the chain, geochemical analysis indicate the restriction of adakitic lavas to Panama (Wegner et al., 2011). Adakite chemistry, associated with slab melt and magmatic contributions from the mantle (Defant et al., 1992), requires tectonically unique conditions that may only be present south of the subducting Cocos Ridge and potentially the formation of a slab window beneath the Chorotega Block (Hidalgo et al., 2009; Mann et al., 2007; Wegner et al., 2011).

There are at least three volcanic centers with Quaternary ages within Panama. El Valle (Wegner et al., 2011), La Yeguada (Knutsen, 2010; Wegner et al., 2011), and Volcán Barú (Camacho, 1998; Knutsen, 2010; Sherrod et al., 2007; UTP, 1992). This investigation focuses on Barú, the westernmost volcanic center in Panama.

Recent Activity

Historic unrest at Barú is limited to an earthquake swarm that occurred beneath the edifice in May 2006 (USGS, 2008) and possible explosive activity at Barú sometime in the 16th century (Montessus de Ballore, 1884; Siebert and Simkin, 2002-). Evidence of Holocene activity also comes from radiocarbon studies at Volcán Barú (Table 2) which delineate 4 periods of volcanic activity within the past 1,600 years (Anchukaitis and Horn, 2005; Behling, 2000; Clement and Horn, 2001; Linares et al., 1975; Sherrod et al., 2007). This

shows Barú may be Panama’s youngest and most likely the center of future volcanism.

Although several authors noted the horseshoe shaped crater and hummocky topography of Barú (Camacho, 1999; deBoer, 1989, Siebert, 2006, Stewart 1978), the report by Sherrod et al., (2007) was first to clearly identify a massive volcanic debris-avalanche deposit described as “the largest example yet documented in Central America” (Sherrod et al., 2007).

TABLE 2 TIMING OF HOLOCENE VOLCANIC ACTIVITY

Volcanic Episode	Time-span	Sample IDs	Source
1	421-544 ybp	VB 88-1	(Sherrod et al., 2007)
		RC 2-3	(Sherrod et al., 2007)
		RC 61-1	(Sherrod et al., 2007)
		Beta 122556	(Anchukaitis and Horn, 2005)
2	600-630 ybp	Beta 95496	(Behling, 2000)
		Beta 150706	(Clement and Horn, 2001)
3	688-953 ybp	Beta 95497	(Behling, 2000)
		VB 93	(Sherrod et al., 2007)
		RC 6E	(Sherrod et al., 2007)
		I-7236	(Linares et al., 1975)
4	1182-1309 ybp	I-7260	(Linares et al., 1975)
		RC 62-1	(Sherrod et al., 2007)
		RC 62-0	(Sherrod et al., 2007)
		Beta 145348	(Clement and Horn, 2001)
		Beta 145347	(Clement and Horn, 2001)

This paper reports field observations and data analysis of Barú’s volcanic debris avalanche deposits and the catastrophic collapse of the volcano’s edifice.

Guiding Questions:

- How many volcanic debris avalanche deposits are attributed to Volcán Barú?
- When did the collapse events occur?
- What are the geotechnical parameters of the deposits and how far did they travel?
- What factors allowed this material to travel across large distances?
- What were the pre-collapse conditions of the volcanic edifice?
- How does the scale and style of Barú's debris avalanches compare with other examples in the geological record?

Terminology

Earliest descriptions of subaerial catastrophic volcanic edifice failure were first conducted on Bandai-san, Japan in 1889; Mageik Islands, Alaska in 1920; Galunggung, Indonesia, 1921; and Raung, Indonesia, 1939 (Griggs, 1920; Neumann van Padang, 1939; Sekiya and Kikuchi, 1889; Siebert, 1996). These sites of collapse are located in regions where multiple failures have now been identified. The 1980 eruption and collapse of Mount St. Helens, Washington was a high-profile event that instigated many changes in geological hazard research and caused major reassessments of volcanic settings (Glicken, 1991). Most of the terms applied in this study of Volcán Barú, Panama come directly from Harry Glicken's work on Mount St. Helens' debris deposits:

Blocks: Pieces of the former volcanic edifice that range from meter-to-centimeter-sizes. They often dominate the interior of hummocks and may be shattered into clasts or preserve original strata. The equivalent of "particle" as defined by H. Glicken, 1991.

Block Facies: The portion of a volcanic debris avalanche that is dominated by blocks; also contains clasts and matrix that may be derived from primary or secondary material.(Crandell et al., 1984; Glicken, 1991; Ui, 1986)

Clasts: The smallest unit of a block; this material dominates the Mixed Facies of a volcanic debris avalanche. Sizes are typically sub-meter. "A rock of any size that would not break if passed through a sieve or immersed in water (Glicken, 1991)."

Disaggregation: “Breaking apart of unconsolidated or poorly consolidated material into its constituent clasts (Glicken, 1991).”

Facies: A term that relates processes to the material as opposed to strict, descriptive nomenclature. For this study, the term is ideal for describing a heterogeneous composition that includes a wide range of particle sizes and allows for a continuum between different textures and composition. Defined as “the lithological, textural, structural and palaeontological features of the sedimentary rock, commonly change laterally as well as vertically in a sedimentary succession. This can involve a change in one or all of the parameters defining the facies. Lateral changes can be very rapid, over several or tens of meters, or more gradational, when the change takes place over several kilometers. Facies change reflect changes in the environmental conditions of sedimentation.” (Tucker, 1996)

Hummocks: Pieces of the former volcanic edifice that were transported relatively intact; “the most characteristic morphologic feature of the debris avalanche deposit;” hummocks are the hilly features that are scattered or clustered on the surface of the runout area (Glicken, 1986, 1991, 1996; Siebert, 1984).

Hummock noise: The population of hummocks representing the smallest, most frequently-occurring hummocks located throughout the VDAD runout area regardless of proximity to the failed edifice. This “noise” was first identified in deposits from Mount St. Helens (Glicken, 1986).

Jigsaw fractures: These are cracks in blocks that have not completely separated the clasts; the pieces could theoretically be fit back together if taken from the outcrop. (Glicken, 1986; Siebert, 1984; Ui, 1983)

Lahar: A hyperconcentrated mudflow that originates from a volcano; also called volcanic mudflows and debris flows. Lahars contain large amounts of water and pyroclastics as primary components. Sedimentary as well as volcanogenic material makes up the secondary components. This material may be deposited many tens of kilometers from the source as it travels down drainage basins. Lahars may be triggered by sudden glacial melt, rainstorms, or dewatering from landslides or sector collapse.

Matrix: The fine material that supports clasts and blocks within the deposit within the Block and Mixed Facies. Grain sizes range from millimeter to microns. Matrix may be found between clasts and blocks and sometimes injected into other strata (as part of clastic dikes) or within the clast or block fractures (often termed “intraclast matrix” see (Bernard et al., 2009; Palmer et al., 1991)) that formed during transport. Matrix dominates the Mixed Facies and often represents the composition of highly disaggregated clasts and blocks.

Mixed Facies: The portion of a volcanic debris avalanche that is dominated by matrix and clasts. “May contain clasts of all rock types and all sizes from microns to meters.” (Glicken, 1991; Ui, 1986) In other studies, is also called the *Matrix Facies* (Crandell et al., 1984; Palmer et al., 1991).

Primary component: Material within a volcanic debris avalanche that originates from the volcanic edifice (lava flows, dome rock, mixed pyroclastics, hydrothermally altered material, etc.). Unlike Secondary Components, this debris excludes all material that was incorporated into the deposit after the collapse was triggered (Palmer et al., 1991).

Secondary component: Material within a volcanic debris avalanche that was incorporated into the deposit during transport. Also termed “exotic,” this material may include: rip-up clasts, volcanoclastic sediments, tuff, peat, lignite, and wood (that may or may not be charred from hot lava blocks) (Palmer et al., 1991).

Shattering: A characteristic often observed in debris blocks; “thorough fracturing of clasts (Glicken, 1991)” that creates angular clasts that may still lie within original block boundaries.

Texture: “Size, shape, and fabric (pattern of arrangement) of particles [blocks and clasts] that form the deposit (Glicken, 1991).”

Toreva block: Similar to hummocks but much larger and do not travel far from the edifice, these are “huge almost intact fragments of volcanic edifices involved in the failure (Ponomareva et al., 2006)” and often appear to have rotated out of position from the flank.(Alverson, 1989; Belousov et al., 1999; Reiche, 1937)

Volcanic Debris Avalanche Deposit: A chaotic, agglomerate deposit resulting from volcanic sector collapse (Siebert, 1984). Often abbreviated as VDAD, DAD, or DA, the composition can be divided into primary and secondary components. Water contained in the material may contribute to fluid-like flow, but the emplacement process is often complex with various styles such as plug flow, laminar, or granular. VDADs may travel for many tens of kilometers from the source and are not confined to drainage basins. Lahars may form from debris avalanche material after or during the emplacement process.

Volcanic sector collapse: A catastrophic form of mass wasting on a volcano; failure of a volcanic edifice; also called a rockslide, landslide, flank collapse, or catastrophic slope failure in other literature but typically involves the mobilization of cubic kilometers of material and removes part of the summit. The motion is mostly lateral as a wedge-like portion of the volcano slides away (Lockwood and Hazlett, 2010; Morelli et al., 2010; Williams, 1941)

Methods

Fieldwork

Field results of this work include estimates of minimum extent and volume of debris avalanche deposit and recognition of two distinct avalanche deposits which substantially overlap each other (Figure 1 and Figure 2). Fresh rock samples were obtained from unweathered exposures. Fieldwork was aided by aerial photos, topographic maps, two digital elevation models (DEMs), and a handheld GPS unit.

The hillshade DEM for Figure 1 and 2 is based on a 30m resolution DEM courtesy from the University of Panama and a 10 m resolution DEM from the USGS. Hummock locations are based on data from field notes, topographic maps, digital elevation models, and 1:20,000 aerial photos. Roads, towns, and rivers have been digitized directly from scanned and georeferenced topographic quadrangles (scale 1:50,000) and only represent a fraction of the detail available from these sheets: 3641-II (Alanje); 3541-I (La Concepción); 3642-III (Plaza de Caisán); 21584 (Bahia Charco Azul); 3742-III (Boquete); 3640-I (Cacao); 3741-IV (Gualaca); 3642-IV (La Unión); 3641-III (Progreso); 3640-IV (Puerto Armuelles); 3640-III (Puerto Limones); 3742-IV (Río Changuinola); 3641-IV (Villa Neily); 3642-II (Volcán)

Quadrangles are published by the Panama National Institute of Geography, Panama City.

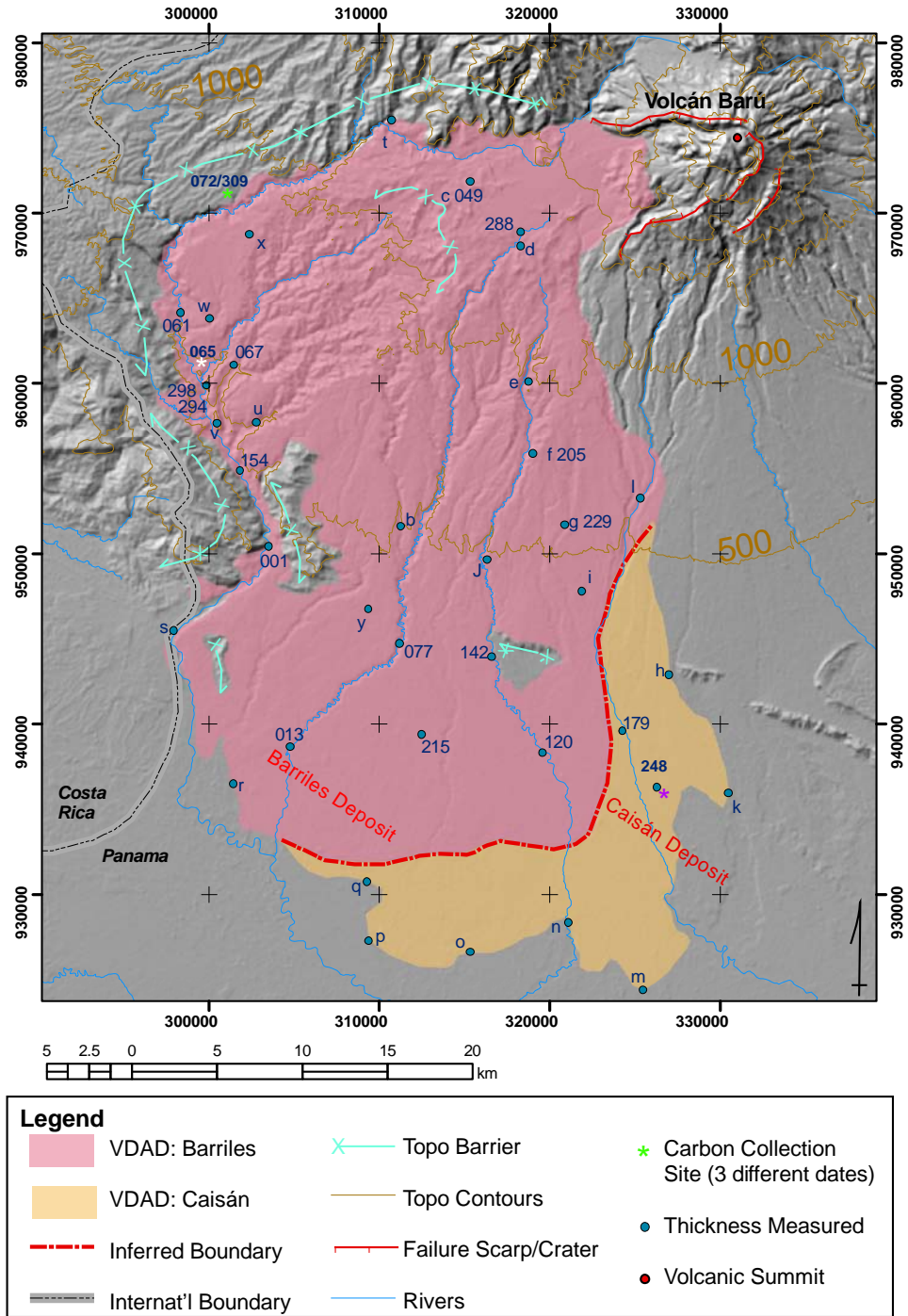


Figure 2 Map of areal extent of the debris avalanches recognized in this study. Note the area of the Caisán deposit includes all the area of the Barriles deposit which it underlies everywhere the base can be examined. The map includes the locations of charcoal dating locations (asterisks; see Table 4 for corresponding values) and depth control points (see Table 7).

Hummocks: Digitizing

Hummocks are the hilly features that make up the rugged surface texture of volcanic debris avalanche deposits. Located around the base of Volcán Barú, these features are sometimes hidden by forested areas but are largely exposed due to land-use practices. Much of the study area contains open pasture and there are many roads (mostly unpaved) that cut across the region allowing good access to the features.



Figure 3 A hummock >5 m in the pasture behind a ~5 m-tall house located in La Meseta less than 5 km north of the Interamerican Highway.

Hummocks are often used for water tower placement and in this region of the study area; many houses are constructed on top of the larger hummocks to take advantage of the views.

Many hummocks were visited in the field and measured directly but due to the large size of the study area, it was more efficient to measure sizes, spatial distributions, and hummock geometries from maps and aerial photographs. The 20 m contour intervals of the topographic maps and the 10 m resolution of the DEM were insufficient to map locations of most hummocks. To address this issue, aerial photos were purchased from the Panamanian Institute of Geography; they were selected to represent the proximal, medial, marginal, and distal zones of the study area.

The 36 aerial photos (27 stereo-pairs) were combined as red/cyan anaglyphs in StereoPhoto Maker v2.32. With 3-dimensional glasses, hummocks were identified by reviewing fieldnote locations and seeking similar

geomorphologies throughout the entire stereo-pair image. Based on scanned and georeferenced topographic sheets, the entire suite of aerial photos was also georeferenced in ArcMap. As hummocks were identified in the anaglyphs, they were digitized by hand in ArcMap as individual polygons.

A total of 4284 polygons were digitized; these shapes represent the planimetric areas of geomorphic features belonging to the volcanic debris avalanche and include toereva blocks as well as large-scale flow structures. Of the total, 4069 of those shapes are interpreted as hummocks. Figure 15 depicts both zones and hummock locations.

Debris Avalanche Deposits

Rarely observed, events that lead to volcanic debris avalanche deposits (VDAD) are catastrophic. One occurring on May 18th, 1980 at Mount St. Helens (Washington, USA) brought worldwide attention and led to discovery of VDADs at several hundred volcanoes. Sector collapses have long recurrence intervals, with a worldwide occurrence of roughly 4 times every 100 years (Siebert et al. 1984) and may occur repeatedly such as Shiveluch, on the Kamchatka Peninsula; Stromboli, Italy; Mount Egmont, New Zealand; and Mombacho, Nicaragua (Belousov et al., 1999; Shea et al., 2008; Tibaldi, 2001; Ui et al., 1986).



Figure 4 A photo cross-section showing the two debris avalanche deposits separated by sedimentary units. GPS site 077 along the Río Gariché (see Figure 2). Upper and lower sections labeled “A” and “C” represent the debris deposits, Barriles and Caisán respectively.

Debris avalanche interiors are exposed in river scarps, road-cuts, and recent quarries. While frequently underlying tephra or fluvium, the Barriles deposit, the younger of the two units, also occurs as the modern surface throughout much of the study area. The Caisán deposit can be seen where the Barriles deposit is deeply dissected (natural and man-made) and often also underlies at least one unit of sediments which occurs between the two debris avalanches (Figure 4). Caisán is assumed to underlie the Barriles throughout its full extent.

Barriles Deposit (VDADII)

The younger of two debris avalanches is here named the Barriles Deposit which occurs in its type section at 8.77 N and -82.80 W (see green asterisk, Figure 2) in a large quarry on the north side of the Río Chiriquí Viejo at 841.5 m elevation. The deposit is exposed in a quarry roughly 100m wide. It contains both a Mixed Facies and a Block Facies. Barriles is the district name for the region that includes Volcán and Nuevo California, towns located at the base of Volcán Barú. Within this district, “hummocky topography” is easily observed and was a principal characteristic of the agglomerate complex identified and named by R.H. Stewart in 1978. Stewart applied the local name, Barriles, likely referring to the archaeological sites where O. Linares and others have studied stoneware and pottery dating from at least 60± 275 B.C. (Adames, 1988).

Represented by 14 samples collected in the field at 13 different locations, the Barriles Deposit is dominated by fine-grained andesitic clasts and blocks ranging in size from gravel to meter-sized found in both, the Block and the Mixed Facies (see summary Table 3). This andesite is typically porphyritic and contains low percentages of vesicles (termed here “dominant andesite”). The mineralogy is represented by the following ranges:

Hornblende: 0-10% black lathes and euhedral crystals up to 6mm – some examples have reaction rims;
Quartz: 0-1% euhedral quartz from 1-2mm;
Plagioclase: 0 - 15% euhedral and lathes from 1-3mm;
Pyroxene: 0-7% from 1-7mm with three exceptional samples that contain 15% pyroxene with 1-3mm crystals (see summary Table 11 in Appendix).
Groundmass: typically dark gray and very glassy, containing microphenocrysts of hornblende and plagioclase with rare quartz and pyroxene.
* Xenoliths of diorite and phenocrysts of completely exsolved, centimeter-sized hornblende minerals are found within 5 different samples.

Block Facies: The block facies is recognized by hummocky surface morphology as well as outcrops that contain more than 30% blocks; block size may be variable and have little-to-intense fracturing (“shattered clasts”). The primary component is volcanic rock; the secondary components include wood fragments (see Figure 12), rip-up clasts of peat, soil, tephra, and volcanoclastics. This is the main facies in the Barriles Debris deposit (Figure 5): blocks often appear as concentrated zones of shattered andesite; large, coherent blocks are only observed where cores of hummocks have been excavated (shallow gravel quarries). Blocks in this facies are supported by matrix. Block Facies that outcrop in the proximal zone (within 20 km of the edifice) typically contain fines of similar composition as the clasts (andesite and dacite) and may be multicolored (e.g. red, purple, orange, gray, and black). Jigsaw fracturing is present in some but not all blocks. No blocks preserving original stratigraphy were observed in outcrop however there was one location where a mafic dike intrusion (~30 cm wide and >5 m long) cuts diagonally through a massive shattered block (GPS 309).

At one outcrop located at GPS 049 a cored hummock is present; the interior has glassy, dense blocks surrounded by shattered, angular clasts of the same lithology. Radial joints in the block suggest thermal stress; thermal

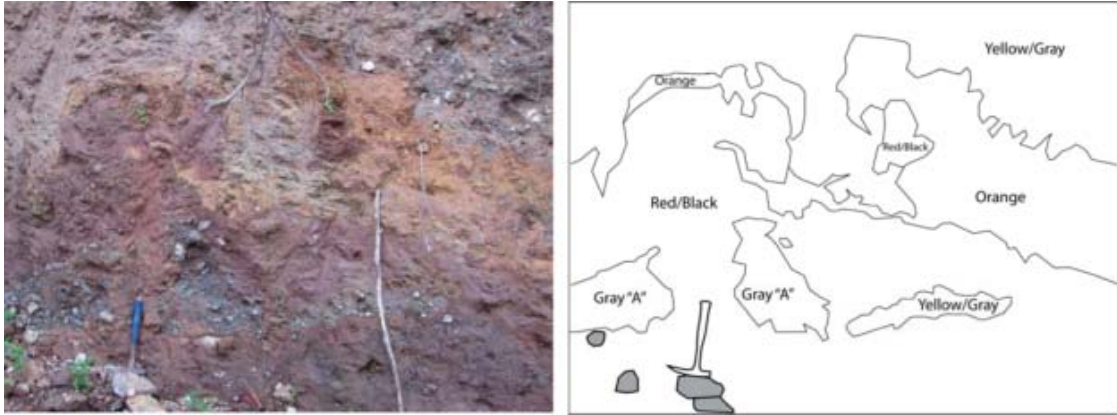


Figure 5 Barriles Deposit Block Facies: At GPS 205 chaotic zones of multicolored material are broken up on a meter-scale showing partial disaggregation of a shattered and smeared andesitic block (Gray “A” and the surrounding “Red/Black” material corresponds with 205B mineralogy) mixed with the block margins. Rock hammer for scale: 32.5 cm.

fractures in the dominant andesite are also observed near GPS 179 in the Caisán Deposit. Andesite is observed in 86% of the exposures sampled for mineralogical description. The surface morphology is rugged with hummocks up to 35 km from the crater; heights ranging from 3 to 96m and spaced 65.2 to 116.3 m apart (see Proximity Values Table 6). The dominant andesite is present as blocks and clasts and is often multi-colored with shades of red, purple, and yellow. Ranging from angular-to-subangular, block sizes range from 0.5 – 15.0m and clast sizes range from 2-26cm. 20 of the 26 rock samples described in Table 13 contain significant concentrations (0-15%) of round-and-merged vesicles.

Mixed Facies: This is located primarily in the marginal and distal zones of the deposit and makes up 14% of the outcrops sampled for mineralogical descriptions. This Facies is recognized by the low concentrations of blocks (<5% of the outcrop) and blocks are often partially-to-completely disaggregated leaving centimeter-sized clasts floating in the fine matrix. The dominant andesite is present as clasts ranging from 2 to 65 cm. Some shattered blocks can be observed in most of the outcrops including jigsaw fractured blocks: 0.2-

2.25 m. From 36 outcrop descriptions, I estimate 10-20% of the mixed facies exposures contain the dominant andesite, up to 60% is composed of yellow-to-orange gray matrix, and 10-20% of the exposure contains other mineralogies and secondary material. Clasts of andesite as well as exotics vary from angular-to-round geometries. The matrix is clay-to-sand sized material that supports the clasts and is also present within fractures and often smeared with the deformed blocks (see Figure 6). Secondary material within the Barriles Deposit includes basaltic-andesite; dacite; hydrothermally altered rock; diorite; rip-up clasts of well-sorted sand, gravel, and clay; humic soil; and wood fragments up to 17cm long.

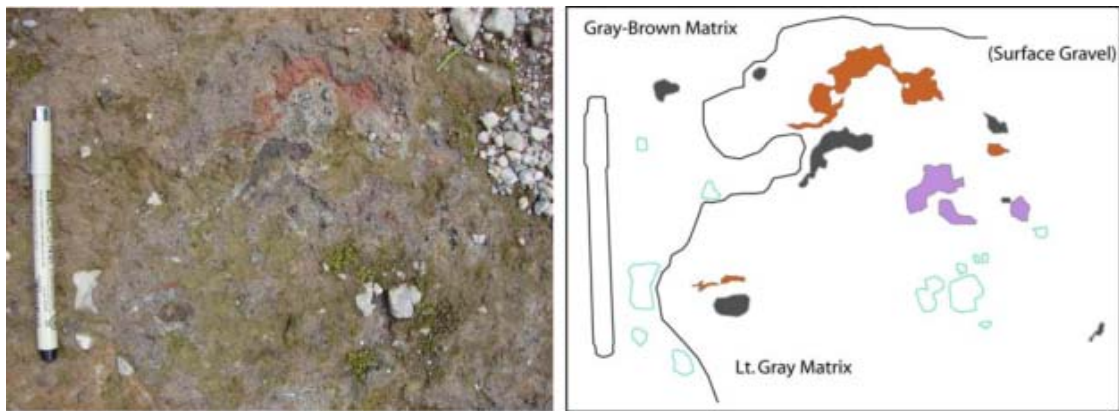


Figure 6 Barriles Deposit Mixed Facies: At GPS 229 showing mixing on a centimeter scale (Length of pen is 13.5cm). Two different matrix materials are present as well as cm-sized clasts of volcanic rock; some are altered to pink and purple while fresh gray and black material is also present.

Caisán Deposit (VDADI)

The older of the two debris avalanches studied is named the Caisán Debris deposit and occurs in its type section at 89.46 N and 103.45E80 W (see white asterisk, Figure 2) in the recently excavated road-cut along the north slope overlooking the Río Caisán at 575 m elevation. At this site, the avalanche outcrops in a >10 m thick exposure and contains both a matrix and block facies. With 12 representative samples collected in the field from 12

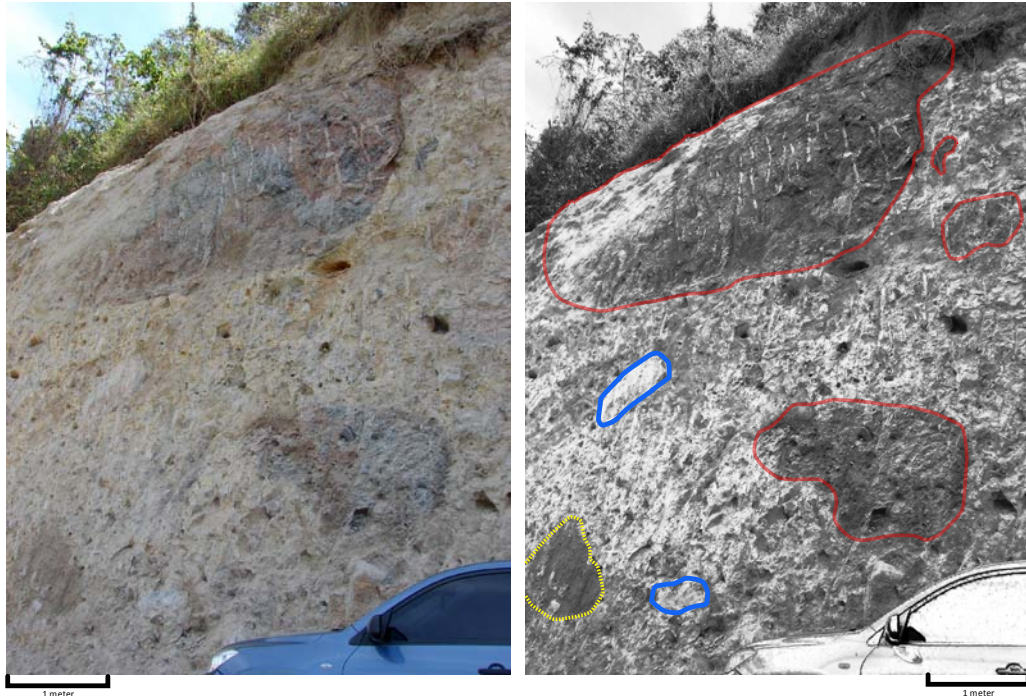


Figure 7 Caisán Deposit Block Facies at GPS 291 (located between 065 and 067 on the map in Figure 2); outcrops along a roadcut leading to Alto de La Mina. This is the type section for the deposit. Red outlines represent the massive, meter-sized debris blocks; Blue outlines are jigsaw fractured clasts of dacite; Yellow outline represents a clast of hydrothermally altered basalt. The scale bar represents 1 meter.

unique sites, the Caisán Deposit is dominated by fine-grained andesitic clasts ranging in size from gravel to meter-sized blocks (see summary Table 3). The mineralogy is typically porphyritic, contains low percentages of vesicles (with two exceptions that contain ~15% vesicles), and is represented by the following ranges:

Hornblende: 0-7% black lathes and euhedral crystals up to 3mm – many examples have reaction rims;

Quartz: 0-3% euhedral from 1-2mm;

Plagioclase: 1- 20% euhedral and lathes from 1-2mm;

Pyroxene: 0-5% from 1-7mm with one exceptional sample that contain ~15% pyroxene with 1-3mm crystals (see summary in Appendix Table 11).

Groundmass: often dark gray containing microphenocrysts of quartz, hornblende, plagioclase, and pyroxene.

* Xenoliths were only observed in three samples but phenocrysts of completely exsolved, centimeter-sized hornblende minerals are found within 3 different samples.

Block Facies: The block facies of the Caisán Deposit was observed in 50% of the outcrops where representative samples were collected. Identification of this facies begins with a block-to-matrix percentage $\geq 30\%$. The typical hummocky surface morphology is often obscured by overlying deposits with the exception of the distal zone that lies within the last 5 km of the runout length. The blocky cores of hummocks located near the termination show layered volcanic units but some dense, glassy andesite cores are also present. The dominant andesite is often multi-colored with shades of red, purple, and yellow. Block sizes range from 0.13 – 4.5 m and clast sizes range from 1 – 30 cm. 3 of the 20 rock samples contain no observable vesicles; otherwise, concentrations range from 1-15%, round-and-merged voids. Four examples of clastic dikes were observed in the field (Sites 301 and 248) and contain fines in lance-like shapes 50-100 cm long and up to 20 cm wide (see Figure 9). The fines and clasts that comprise the matrix of the Block Facies are noticeably weathered in comparison with the matrix in the Barriles Deposit; they appear pale to bright yellow and many clasts have weathered rinds.

Mixed Facies: It outcrops primarily in the marginal and distal zones of the deposit and is represented by half of the samples collected in the field. The surface is only exposed in the distal zone (see Figures 1 and 2). The Mixed Facies contains $< 5\%$ blocks with characteristically small hummocks. In the distal zone, where surface features are present, hummocks are scattered with heights ranging from 3 to 5 m typically spaced 204 m apart (see Proximity Analysis Table 6). The dominant andesite is present as clasts ranging from 10 to 40 cm. Some shattered blocks can be observed in most of the outcrops



Figure 8 Caisán Deposit Mixed Facies: At GPS 246, meter to submeter-sized blocks (rock hammer for scale, 32.5cm) outcrop in an excavation site >21m deep. Two varieties of blocks are represented here: Blue outline indicates the jigsaw fractured clasts of andesite; Red outline marks hydrothermally altered basalt; Orange region is smeared humic soil.

including 0.4-3.0 m jigsaw fractured blocks. While 10-30% of the exposures contain the dominant andesite, up to 60% is composed of yellow-to-orange gray, matrix.

The matrix of Caisán's Mixed Facies is clay-to-sand sized material that supports the clasts and is also present within fractures and often smeared with the deformed blocks (see Figure 8). Clasts of andesite as well as exotics vary from angular-to-round geometries. Up to 30% of the exposures consist of miscellaneous volcanic lithologies and secondary material including: basaltic-andesite; dacite; hydrothermally altered rock; diorite; limestone; schist; rip-up clasts of well-sorted sand and gravel; gray and a distinctive green clay; humic soil; and wood fragments up to 45cm long.



Figure 9 Caisán Deposit: a clastic dike cuts near-vertically through a pervasively fractured (also highly altered) debris block at GPS 294. Out of view to the right are two more similar features with the same trend. Rock hammer centered in view for scale: 33cm.

TABLE 3 CLAST AND BLOCK VALUES

	GPS ID	Deposit	Facies	Clast Size	Block Size
1	42	Barriles	Mixed	5-65cm	1-2m
2	58	Barriles	Block	5-18cm	10m
3	106	Barriles	Mixed	2cm	2m
4	111	Barriles	Block	3-26cm	15m
5	Escárrea*	Barriles	Mixed	3-8cm	0.5m
6	142	Barriles	Block	2-8cm	0.6m
7	148	Barriles	Mixed	2-15cm	0.2m
8	013B	Barriles	Mixed	15-60cm	0.9m
9	179	Barriles	Mixed	10cm	1-2m
10	227	Barriles	Mixed	7cm	0.5m
11	228	Barriles	Mixed	5cm	0.45m
12	246	Barriles	Mixed	5-7cm	0.4-0.6m
13	274	Barriles	Mixed	10-30cm	2.25m
14	33	Caisán	Mixed	30cm	3m
15	163	Caisán	Block	1-10cm	0.2-1.0m
16	164	Caisán	Block	20-30cm	1m
17	168	Caisán	Block	4cm	0.13-0.18m
18	013A	Caisán	Mixed	15-40cm	2m
19	290	Caisán	Mixed	10-18cm	0.4-1.25m
20	298	Caisán	Mixed	10-30cm	0.75m

* This site is located at a bridge crossing of the Río Escárrea, also known as the Río Guigala; coordinates in UTM NAD27 17P 319150/939200.

Sedimentary Architecture



Figure 10 Upper contact of the Caisán Deposit in the distal zone. Pink fines with pumice fragments and pale gray fines overlie the debris avalanche. Pen for scale (13.5cm).

The internal structures of both the Barriles and Caisán Deposits are distinctively chaotic. There are no outcrop exposures exhibiting imbrication or sorting and the transition between Block and Mixed facies is gradational. Within both facies, blocks are typically fractured and often disaggregated at the margins; matrix material can be observed between the peripheral clasts. Clasts of pervasively fractured andesite as well as clasts of secondary material have been observed with intra-matrix material. Partly disaggregated blocks sometimes exhibit boudinage and smeared structures as opposed to simple shearing but isolated jigsaw fractured blocks appear throughout the deposits in the medial and distal zones (example from distal Caisán, Figure 8).

In the stratigraphy there are conforming units lying in-between the VDADs; they have a thickness range of 0.3 to 3.0 m. These deposits are not indurated and consist of paleosols, moderately-to-well sorted fluvial deposits, and two thin (65 cm and 80 cm respectively) layers of fines interpreted here as pyroclastic deposits (GPS 248, see Figure 10). These deposits of fines included small porous grains as well as

rounded clasts of altered material incorporated into the upper section of the Caisán Deposit. Upper and lower contacts with these intermediate deposits are

typically sharp and planar except for the few exposures of Caisán's basal contact. Basement rock is observed partly incorporated into the lower section of the Caisán Deposit at GPS 067. In the proximal zone, the surface of the Barriles Deposit is exposed as hummocks; the inter-hummock areas are blanketed by fine, white tephra, soil (GPS 288 Figure 11), and within 5 km of the breached crater, block and ash units with entrained charcoal can be observed in recent, shallow quarries.

Summary of field characteristics

The Barriles Deposit is best characterized by the hummocky topography found at Barú's base and is dominated by fresh-looking andesitic blocks. Pristine andesite is present and contains very small, round vesicles suggesting dome rock; brilliantly colored clasts were likely formed by hydrothermal alteration. The recently emplaced debris avalanche is also surprisingly



Figure 11 Upper contact of the Barriles Deposit within 10km of the breached crater. At GPS site 288, the Barriles Deposit is covered by two thin (60cm and 17cm respectively) beds of volcanic ash with an intervening layer of soil (70cm). At the right-hand side a rock hammer for scale (32.5cm).

fragmented. Distinctive jigsaw fractures and densely shattered blocks are well-distributed throughout the deposit: within the tall hummocks of Volcán and Cuesta de Piedra (GPS points 049 and 229) as well as tens of kilometers south near the town of La Concepción (GPS points 077).

The Caisán Deposit typically occurs beneath the Barriles Deposit. Evidence from this investigation shows that Caisán travelled further and its surface is only exposed in the most distal regions at the south and east edges of the study area. The hummocks from this deposit are similarly shaped and generally clustered, but they are smaller and geomorphologically more subdued than Barriles hummocks. No exposures of proximal hummocks exist for the Caisán, but comparing the distal hummocks of both deposits shows deep hydrothermal alteration and the block facies is generally more weathered – even the most fresh-looking shattered blocks show oxidation along joints and fracture margins within the Caisán Deposit.

The two collapse events incorporated very similar material; without field correlations and clear contacts between the deposits, the Caisán and Barriles Deposits often appear identical. This is especially true for the Mixed Facies where fines, clasts, and fractured blocks are often identical in composition, size, geometry, and quantities. Mixed Facies blocks found within the Caisán Deposit are often larger than those within the Barriles Deposit, but the shattered nature of the material makes exact measurements difficult. Within the Block Facies, sizes are reversed: the Barriles Deposit contains blocks up to 15 m long; the Caisán contains blocks up to 4.5 m. The variety of lithologies of secondary components aids distinguishing the two deposits, but careful observation is necessary in order to find the hallmark clasts of limestone, schist, and green clay. The dominant andesite found in both deposits appears identical in hand



Figure 12 Charred wood within the Barriles Deposit Type Section.

At GPS site 072, this is the type section for the Barriles Deposit. Located within a large (100 m wide) active quarry, the Block Facies is exposed with highly fractured clasts dominating the shear walls of the quarry. This photo is focused on the inter-block matrix where cobble-sized clasts of andesite are mixed with gray and pink fines. The fine material appears to be pulverized andesite and surrounds a broken piece of wood (a 10cm cross-section is just left of the trowel when the wood was removed it was a total of 17cm long). The wood is blackened on all surfaces and provides the date appearing in Table 4. A 20cm trowel in view for scale.

sample. A second common rocktype in both deposits is pyroxene-rich andesite which is scattered throughout the deposits. This is potentially the same lithology mapped and sampled from the “old dome” within Barú’s craters (Sherrod et al., 2007).

From the above descriptions I infer that both of these debris avalanches were similar events, primarily derived from an unstable, hydrothermally altered, generally homogeneous volcanic dome complex that formed above the vent at Barú. Field observations and measurements of blocks characterize both deposits as having relatively large volumes of dome material suggesting that Barú was extruding tens of cubic kilometers before catastrophic flank collapse occurred. Since the last collapse, at least 10 km³ of dome material has refilled the horseshoe-shaped crater (Sherrod et al, 2007).

Radiocarbon Dating

Carbon material was collected from 6 locations and 4 samples are dated here (Figure 2 shows sample sites and Table 4 follows with lab results). These were submitted to Beta Analytic and corrected using OxCal 4.1 with the INTCAL09 database. Ages are reported as years before 1950 A.D. at the 2 sigma confidence level. Calibration plots are included in the Appendix, Figure 30.

The carbon samples were taken from entrained charred wood fragments and humic soil. This analysis provides the lower limiting ages for the debris deposits. Two samples were taken from the Barriles Deposit, from the same quarry at GPS 309 and 072 (the type section location, Figure 2). The combined and calibrated age is 9250 – 9020 years before present placing it in recent geologic time. The two samples from the Caisán deposit were taken from two separate locations: sample 065 is from the medial zone and sample 248 is from the distal zone. The former sample provided an age very close to the limit of radiocarbon analysis, 48,636 – 45,224 while the latter sample yielded no age as it was beyond the range of radiocarbon. Both samples from Caisán were competent wood fragments (one showed blackened surfaces along all of the ragged surfaces) but the lab results suggest that this deposit cannot be dated with radiocarbon methods and the result from 065 could reflect minor contamination from other carbon sources. I conclude that Caisán event is older than 45,000 years before present.

TABLE 4 RADIOCARBON AGES FROM VOLCÁN BARÚ'S VDADS

#	Deposit: ID	Coordinates(UTM) UTM WGS84, Zone 17	Radiocarbon Age (+/- 2 sigma)	Calibrated Ages (BP)
1	Barriles: 072	301673 970533	8000 ±30	9006 – 8764
2	Barriles: 309	301601 970332	8590 ±50	9671 – 9490
3	Caisán: 065	300714 960829	43,350 ±750	48,636 – 45,224
4	Caisán: 248	326301 936025	NA	>43,500 BP

Notes: The collection locations (Figure 2) of the two Barriles samples come from the same quarry (green asterisk), Caisán 065 (white asterisk), and Caisán 248 (pink asterisk). Weighted average for 1 and 2: 8169 ±26 BP and Calibrated Range: 9250 – 9020 BP Reference: (Bronk Ramsey, 2009)

Carbon Sample Descriptions:

- 1: Charred wood fragments found 27 m below the top of a thick section of matrix-supported debris avalanche in a quarry near San Antonio, north of Río Chiriquí Viejo.
- 2: Charcoal taken 27 m below the top of a thick section of matrix-supported debris avalanche in a quarry near San Antonio, north of Río Chiriquí Viejo (same quarry as “072”).
- 3: Wood fragments taken 15 m below the top of a thick section of matrix-supported debris avalanche in a roadcut near Bajo de la Mina.
- 4: Wood fragments from entrained sediment found 10 m below the contact in a thick section of fines-rich debris avalanche in 21 m deep construction site south of the Interamerican Highway.

Hummock Geometry and Distribution

In the field, hummocks appear as rounded, hilly features, often clustered together and often with rocky surfaces. For this reason, distinguishing hummocks is a subjective process. Similar geomorphological features are present in this field area, but they lack the surface texture, symmetry, and scale that make hummocks unique. Old stream meanders, peaks between drainages, flow structures from pyroclastic material, and anthropogenic

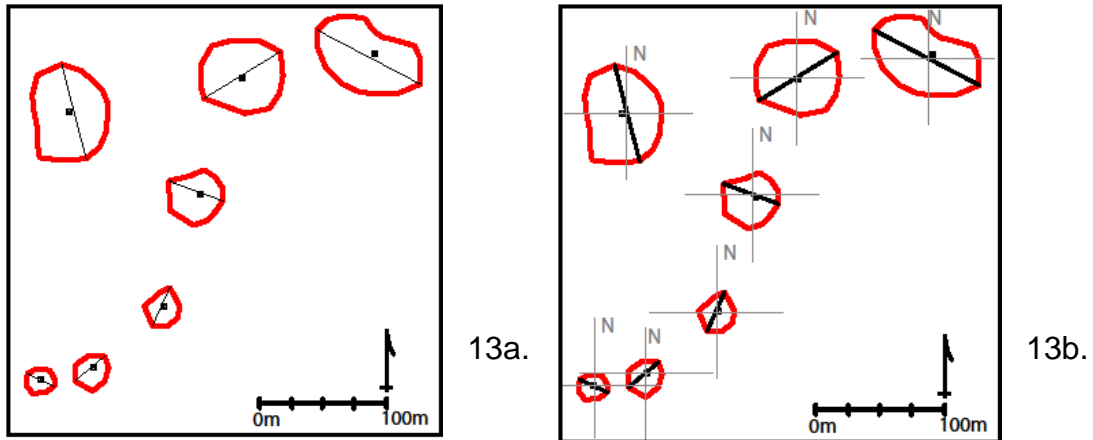


Figure 13 Examples of polygon geometries. In 13a. the long axis (black lines) and centroids (black circles) of each hummock (red polygons) are analyzed with geospatial software. In 13b. the azimuth with respect to north (gray lines) is calculated with a MatLab script.

structures were identified and excluded from hummock analysis. Also excluded are avalanche flow structures and toreva blocks, features present in zones closest to the presumed source of material. Hummock geometry and distribution was investigated using geometric parameters such as diameter, area, orientation. Interhummock distances may relate to coverage area, population concentrations, regional slope, and runout distances. Digitized hummock data was divided into six groups based on spatial positions (Figure 15).

Due to the dispersed nature of the hummocks and the numerous datapoints, spatial analysis based on aerial photos was analyzed instead of relying entirely on field observations. Digitized in ArcMap, more than 4,000 polygons representing hummocks were assessed with a script written in MatLab v.7.10.0; this measured the most distal vertices of each shape and their direction from north. Results are treated statistically zone-by-zone and grouped in order to distinguish data trends.

TABLE 5 HUMMOCK STATISTICS ZONES 1-6

Row #	Description	Z1	Z2	Z3	Z4	Z5	Z6
1	Hummock Count	976	477	993	521	538	565
2	Coverage area within VDAD, km ²	151.1	39.5	31.9	42.5	49.5	75
3	Hummocks per km ²	6.5	12.1	31.1	12.3	10.9	7.5
4	General slope, from N-S (degrees)	-1.3°	-4.2°	-2.5°	-2.2°	-0.9°	-0.8°
5	Area of largest hummock, km ²	0.760	0.081	0.066	0.076	0.016	0.034
6	Diameter of largest hummock, m	1545	470	510	430	222	353
7	Area of smallest hummock, m ²	94.2	82.11	71.4	189.5	137.9	59.1
8	Diameter of smallest hummock, m	13	10	10	20	16	12
9	Orientation (modes of azimuths)*	SW	SE	SE,SW	SW,SE	SE,SW	SE,SW

* Directions were determined from Rose Diagrams plotted in Figure 32 in the Appendix.

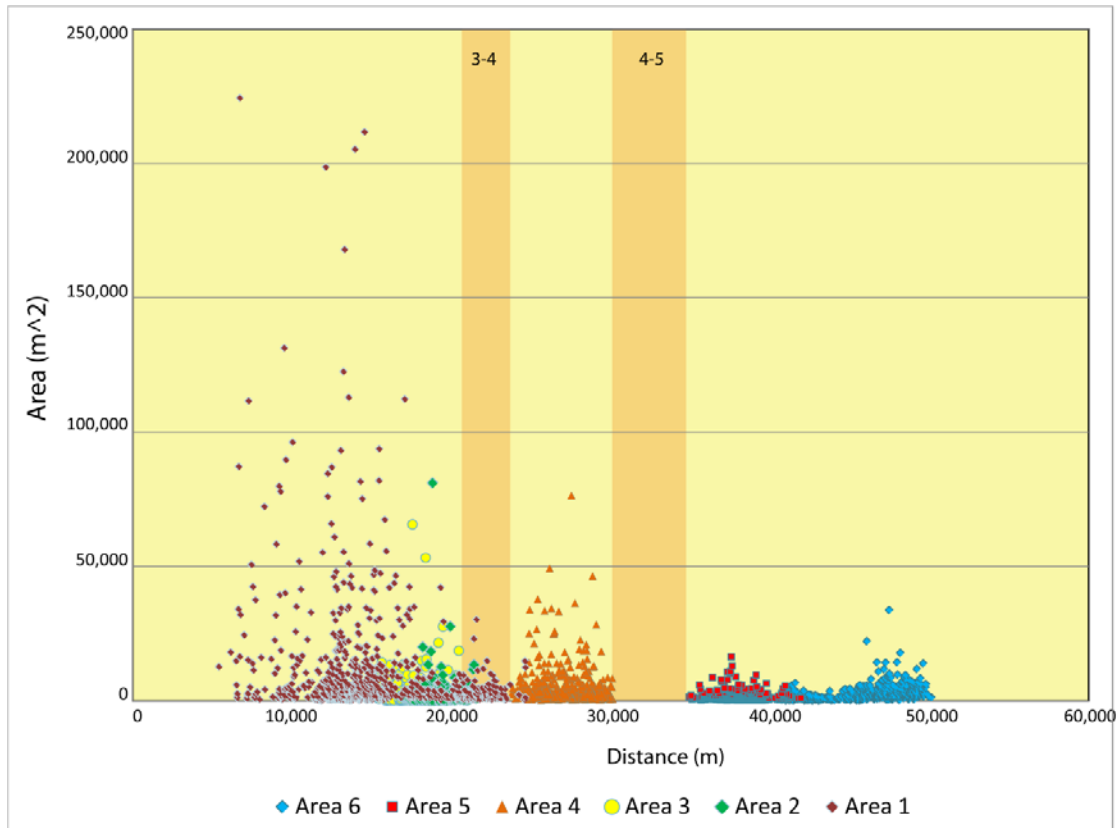


Figure 14 Entire field area: Hummock Area vs. Distance (in meters). Orange bars represent data gaps where no aerial coverage is available: Between Zones 3-4 and 4-5.

Hummock area vs. distance is plotted in Figure 14. Zones from Table 5 are plotted in separate colors and data gaps are represented by vertical bars on the plot. Most hummocks are smaller than 50,000 m². Larger hummocks tend to occur closer to the source and the maximum decreases with distance. There are some anomalies in this overall trend.

Hummock orientations (*Row 9* in Table 5) may relate to how the deposits came to rest. Reading North as “0” and South as “180,” the frequently occurring long axis directions indicate bimodal distributions. Values from the whole dataset are plotted in Figure 32 (see Appendix). Here we see high frequencies between 45-30° and 150-120°.

Hummock Proximity

Inter-hummock distances were also analyzed. Digitized polygons were used to determine the distances between centroids of each shape. In ArcMap the “Generate Near Table” function creates pairs for all points. Pairs are defined as closest points and the program measures the distances between them. For each Zone, the pair with the largest distance is reported. The mean distance is also calculated and reported in Table 6 below.

TABLE 6 HUMMOCK PROXIMITY VALUES

Zone	Hummocks Population	Maximum distance, m	Mean distance, m
1	976	1414.7	116.3
2	477	234.5	70.0
3	993	232.3	65.2
4	521	397.5	110.9
5	538	882.6	108.6
6	565	780.9	204.8

Results from the proximity analysis show that the size of each hummock population has no impact on the maximum or mean values. Results from the maximum distance analysis are inconclusive but the mean distance analysis reflects a similar trend to large hummock sizes recorded in Table 5. Focusing on the mean values we see a decrease from the proximal area (Zone 1) until the medial zone (here Zone 4 increases by more than 45 meters). Distance values decrease slightly in the next Zone but the last Zone shows a sudden increase (just like hummock diameters and areas in Table 5).

In summary, my investigations of digital hummock polygons show a trend correlating hummock location with size and distribution. Results show that large area and diameter hummocks are located in the zones of widest mean

distribution (proximity). Where regional slope is greater, more hummocks are observed and are larger than other parts of the runout area. Regional slope also affects the orientations of the hummocks and causes stronger unidirectional alignment where slope is higher.

The termination of the debris deposits and the effects of the subsurface are reflected in hummock distribution. Zones 5 and 6 cover the runout of the Barriles deposit and the slightly longer extent of Caisán. Hummocks are more spread out but larger in Caisán's distal zone. Midway through the runout area there is a sudden increase in hummock sizes (area and diameter); this is observed primarily in Zone 4. Interhummock distances also suddenly increase in this same area. The unique location is coincident with the emergence of confining topography. The ridgeline Cerro Sortová cuts through the debris avalanche deposits directly below Zone 4. Topographic barriers also appear immediately southwest in the region dominated by Cerros Machuque (more than 100m taller than surrounding topography). These features may have caused the debris avalanche to funnel through this area during emplacement. The avalanche would have been slowed down and coherent portions of the VDAD collected or stalled as the avalanche moved en masse across the runout area.

Data from other debris avalanche deposits suggest that a distinctive toe may form at the distal edge. This is a primary feature in VDADs that are valley confined such as Mount St. Helens, Socompa, and Shiveluch (Belousov et al., 1999; Belousov, 1995; Glicken, 1986; Major and Iverson, 1999; Ui et al., 2000; Wadge et al., 1995) and is not observed in Barú's deposits. If catastrophic flank collapse occurred as a series of failures, debris may travel and spread as separate lobes with variable hummock sizes regardless of proximal, marginal,

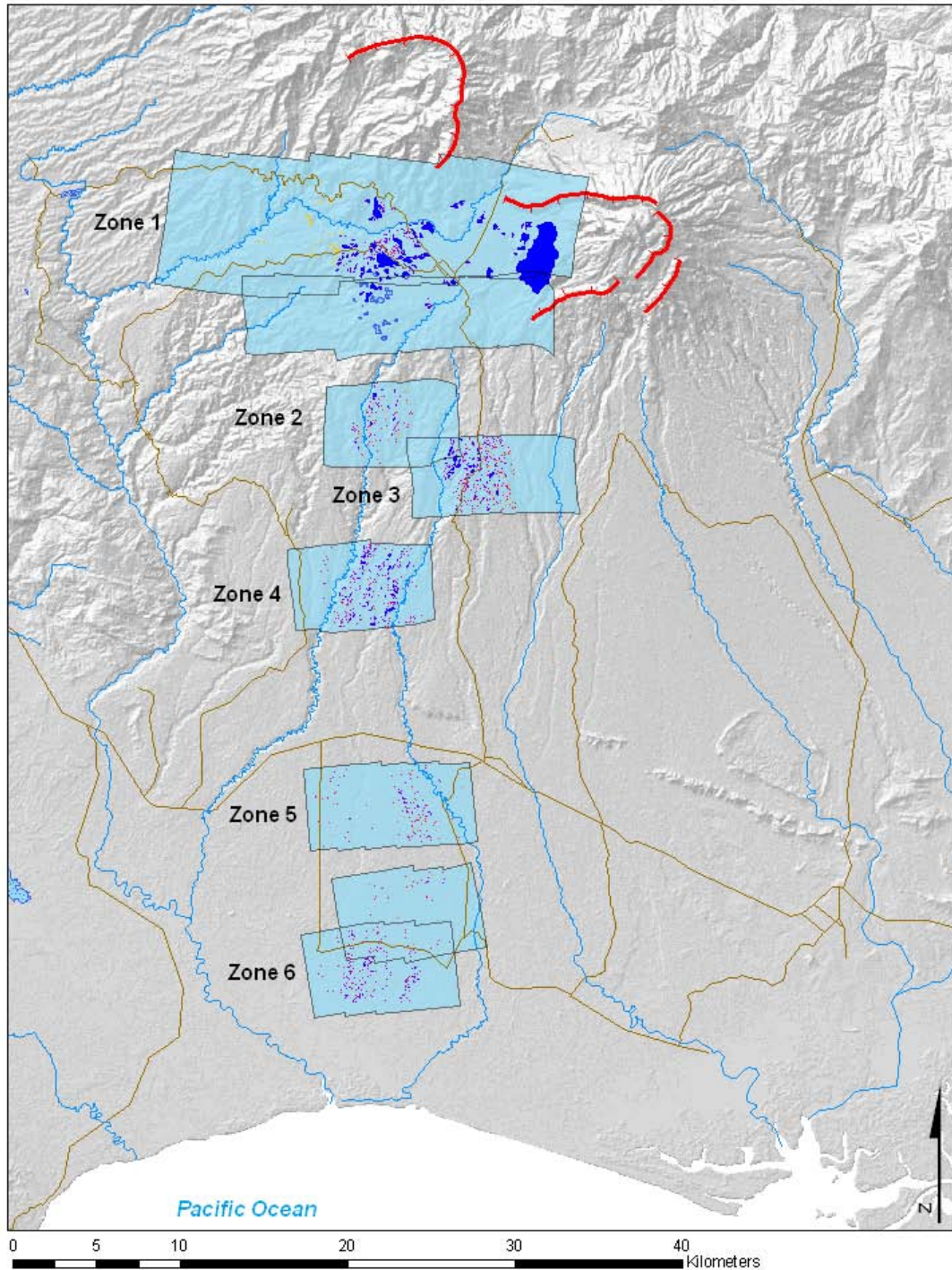


Figure 15 Zones of aerial coverage and digitized hummocks. Key: Red = smallest hummocks; Blue = largest hummocks. The proximal torevia block is the largest blue polygon; Light blue rectangles = aerial photo coverage; Blue Lines = Rivers; Brown Lines = Roads; Red Lines = Volcanic Craters.

medial, or distal conditions (this is observed at Shiveluch Volcano, see Belousov et al. 1999 and scaled experiments in Major and Iverson, 1999).

The hummock datasets were analyzed independently from facies and unit descriptions. The contacts for the Barriles and the Caisán Deposits were drawn based on final analysis results as well as outcrop observations (see geologic map, Figure 1). While there is no topographic expression of a toe, field observations and hummock trends indicate where the contact is located.

Volume Calculation: Deposit Thicknesses

To estimate the volumes of Volcán Barú's debris deposits, thickness data was collected in the field from 12 locations (Table 7, Figure 2). To provide better area estimates, 25 additional points (IDs b through y) were inferred based on proximity to measured outcrops, maximum heights of nearby river scarps, and a tomography report developed by ADGEO for a hydroelectric company (AdGeo, 2008).

Heights of river scarps were estimated with cross-sections from topographic profiles across the Río Chiriquí Viejo, Río Pavón, and two regional profiles. A rafting trip on the Río Chiriquí Viejo (Figure 2; GPS Points 154 to 001) allowed views into the stratigraphy but direct measurements could not be taken from the moving raft. An important feature observed on that traverse was the natural tendency of the river to scour and cut terraces at the contacts between the basement rock and the debris avalanche and along intermediate terracing where the Barriles and Caisán deposits are in contact. This terracing possibly reflects the ability of the river to cut down through variable materials. The profile tool in Global Mapper drawn across the 10m DEM retrieves 3 values: Water level, middle contact, and the modern surface "maximum." The

middle contact thus possibly reflects contacts between the two debris avalanche units.

The point data tabulated on the following page can be used to create Voronoi Polygons and create divisions for thicknesses based on geometrical relationships (see Figure 16). Voronoi Polygons (also called Thiessen cells) are drawn based on shared intersections that are the closest points to a node; in this study, the nodes are the thickness points and bound by the mapped extent (Chang, 2006). Using Spatial Analyst tools in ArcMap 9.3, a coverage layer was created for both debris avalanche deposits. The 37 unique thickness values and aerial coverage of the Barriles and Caisán Deposits required separate calculations to determine debris avalanche volumes. These volumes are reported in Table 8.

TABLE 7 (NEXT PAGE) THICKNESS POINTS

Used in estimates for debris avalanche volume determinations. Locations of ID points are shown in Figure 2. Many are located at the edges of the deposit and are assumed to be thin (bounding limits).

* Calculated from topographic cross-sections.

** Base is not exposed, rounded value.

Note: AdGeo refers to a geotechnical report prepared during a geophysical investigation for the Río Piedra/Chico hydroelectric dam construction (AdGeo, 2008). The following ranges were reported:

Barriles range = 4.4m to 35.4m; reported average = 20.0m

Caisán range = 17.8m to 39.4m; reported average = 28.6m

TABLE 7 VOLCÁN BARÚ DEPOSIT THICKNESS POINTS

Barriles Deposit			Caisán Deposit		
ID	Thickness (m)	Source	ID	Thickness (m)	Source
001	38.0	Inferred	001	91.0	Inferred
298	1.3	Outcrop	298	28.6	From AdGeo **
294	3.4	Outcrop	294	28.6	From AdGeo **
246	3.5	Outcrop	246	28.6	Outcrop**
215	16.5	Outcrop**	215	39.4	From AdGeo
154	188.0	Inferred *	154	97.0	Inferred *
142	15.0	Outcrop	142	28.6	From AdGeo
120	8.0	Outcrop	120	28.6	From AdGeo **
077	2.0	Outcrop	077	39.4	From AdGeo **
067	5.0	Outcrop	067	28.6	From AdGeo
061	16.5	Outcrop	061	28.6	From AdGeo
072	8.0	Outcrop	072	28.6	From AdGeo **
309	35.0	Inferred *	309	40.0	Inferred *
b	90.0	Inferred *	b	65.0	Inferred *
c	97.0	Inferred *	c	99.5	Inferred *
d	90.0	Inferred *	d	80.0	Inferred *
e	40.0	Inferred *	e	95.0	Inferred *
f	35.4	Inferred *	f	40.0	Inferred *
g	20.0	Inferred *	g	40.0	Inferred *
h	4.4	Inferred *	h	17.8	From AdGeo
i	20.0	Inferred *	i	28.6	From AdGeo
j	1	Bounding limit	j	17.8	From AdGeo
k	1	Bounding limit	k	1	Bounding limit
l	1	Bounding limit	l	1	Bounding limit
m	1	Bounding limit	m	1	Bounding limit
n	1	Bounding limit	n	1	Bounding limit
o	1	Bounding limit	o	1	Bounding limit
p	1	Bounding limit	p	1	Bounding limit
q	1	Bounding limit	q	1	Bounding limit
r	1	Bounding limit	r	1	Bounding limit
s	1	Inferred *	s	1	Inferred *
t	69.0	Inferred *	t	86.0	Inferred *
u	5.0	Inferred *	u	40.0	Inferred *
v	20.0	Inferred from quarry depth	v	40.0	Inferred from quarry depth
w	40.0	Inferred from RCHV	w	60.0	Inferred from RCHV
x	35.0	Inferred *	x	50.0	Inferred *
y	20.0	Inferred *	y	40.0	Inferred *

Using polygons does not create a smooth, realistic surface but may be a good 1st order minimum estimate of thickness and resulting volumes. To model more natural terrain, the point data was interpreted as isopachs and contoured in smooth curves following inferred pre-emplacment conditions. The contours were interpolated to a raster to create DEMs. This method results in higher volume estimates for the two deposits (see Table 8).

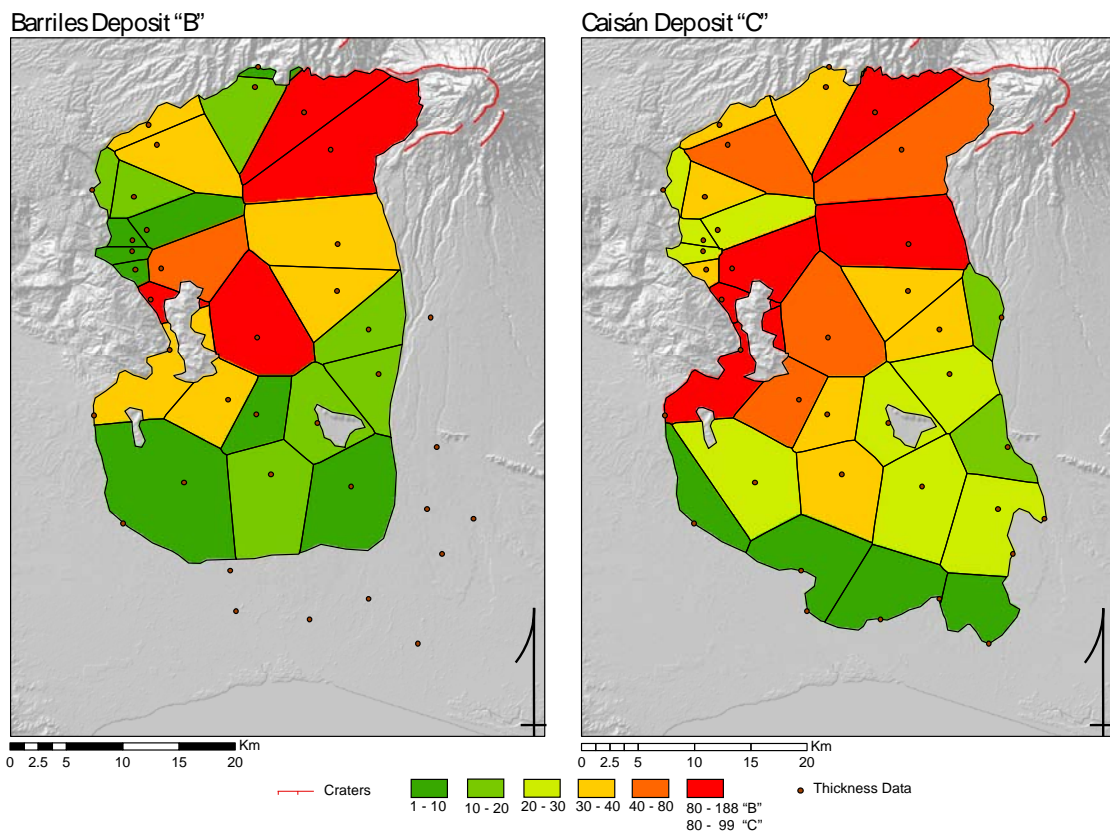


Figure 16 Thickness polygons of Barriles (left) and Caisán Deposits (right). These polygons represent unique thicknesses which are multiplied by respective areas to compute an aggregate volume for the deposits. Each polygon is controlled by a thickness estimate and the polygon shape is determined by the other points that are nearby using the Voronoi process (Chang, 2006). Thickness units in meters.

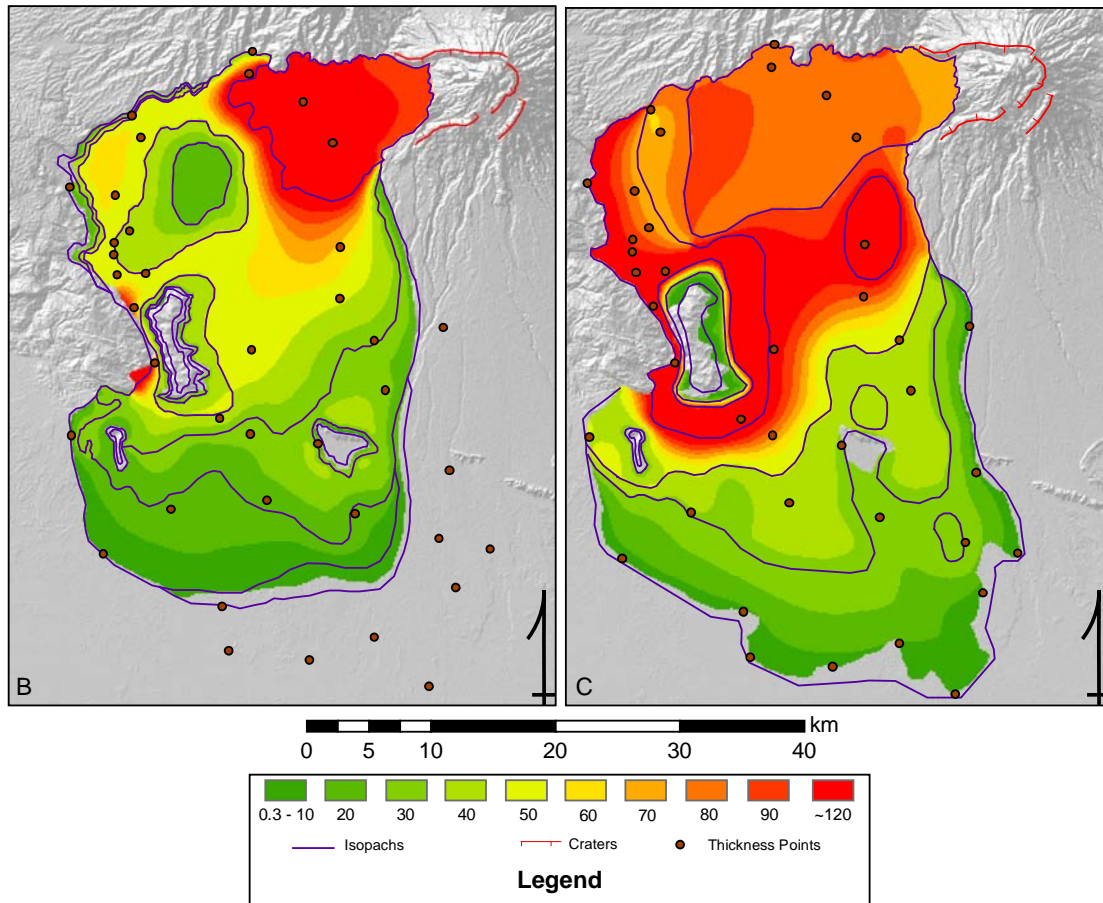


Figure 17 The Barriles (left) and Caisán Deposit (right) volumes as measured by isopachs and a continuous, smooth surface from a DEM. Thickness in meters.

Volume Calculations: Edifice Reconstruction

The current horseshoe-shaped crater of Volcán Barú suggests that a large volume of material is missing from the edifice. The rough outline of the crater is actually a series of segments interpreted as failure scarps. An alternative method for determining debris volumes is to complete the contours of the failed edifice (Sherrod et al., 2007). This process attempts to reconstruct the precollapse conditions at the volcano.

The first step was to define the maximum limit of the Barú edifice. I used a 10 m DEM created by the USGS from digitized clear film separates of 4 quadrangles with 20 m contour intervals. A 28x25 km area (712 km²) centered

on Barú was clipped and assumed to represent the proximal and edifice region. The N-S and E-W cross-sections of the volcano determined a primary break in slope at the 1,300 m contour. That slope intersection is assumed to define the southern and eastern limit of the edifice. A raster of the slope created in ArcMap shows a transition at the 6.5° limit on the western edge of the proximal zone (Figure 18). The northern extent is well-defined by the older topography of the Central Cordillera. With these considerations combined with field observations of the geomorphology (e.g. where the toeva block terminates and where the hummocks begin) the edifice is distinguished from the ring plain (Hackett and Houghton, 1989).

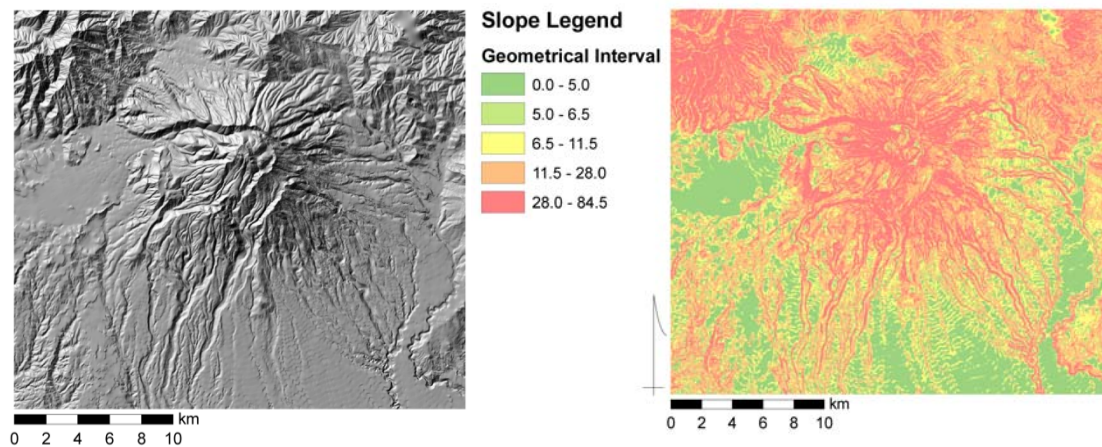


Figure 18 Left: 10 m DEM of the Volcán Barú region. Right: Slope map of the region based on 5 Classes with rounded Geometrical Intervals of increasing slope: 5.0°, 6.5°, 11.5°, 28.0°, 84.5° chosen to represent the most dramatic changes in slope.

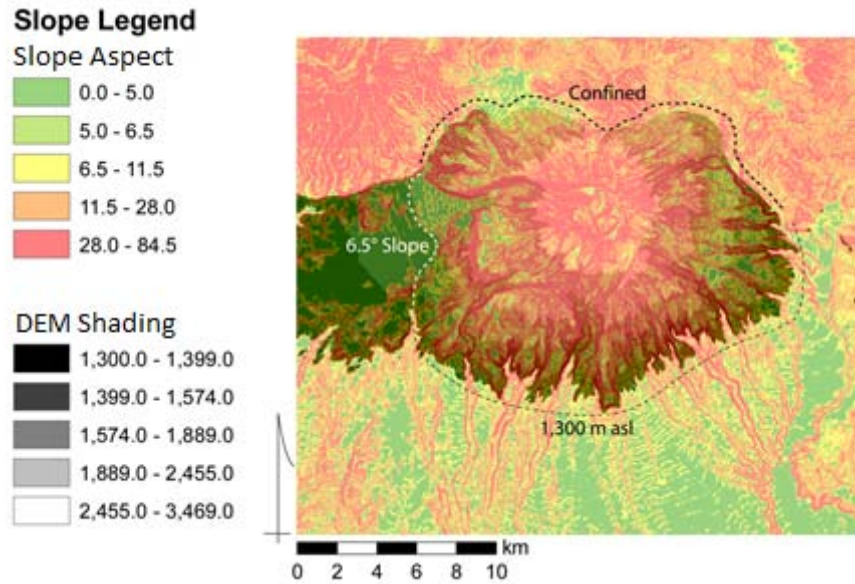


Figure 19 Edifice zone is digitized based on elevation, slope, surface texture, and field observations: Heavy Black Dotted Line = Northern limit determined by confining topography; Thin Black Dotted Line = Southern and Eastern limit defined by 1,300 m above sea level contour line; White Dotted Lined = Western limit defined by the $\geq 6.5^\circ$ slope and field observations.

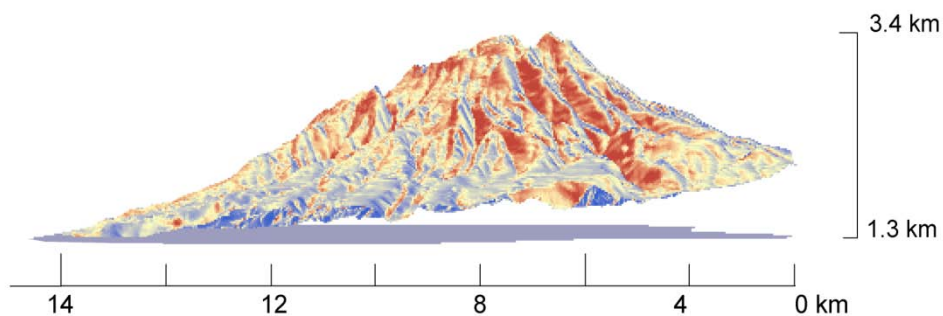


Figure 20 Barú's current edifice; view directly North. Displayed in ArcScene 9.3, the clipped DEM with a 235 km² horizontal footprint (blue-gray shadow) and 2x vertical exaggeration.

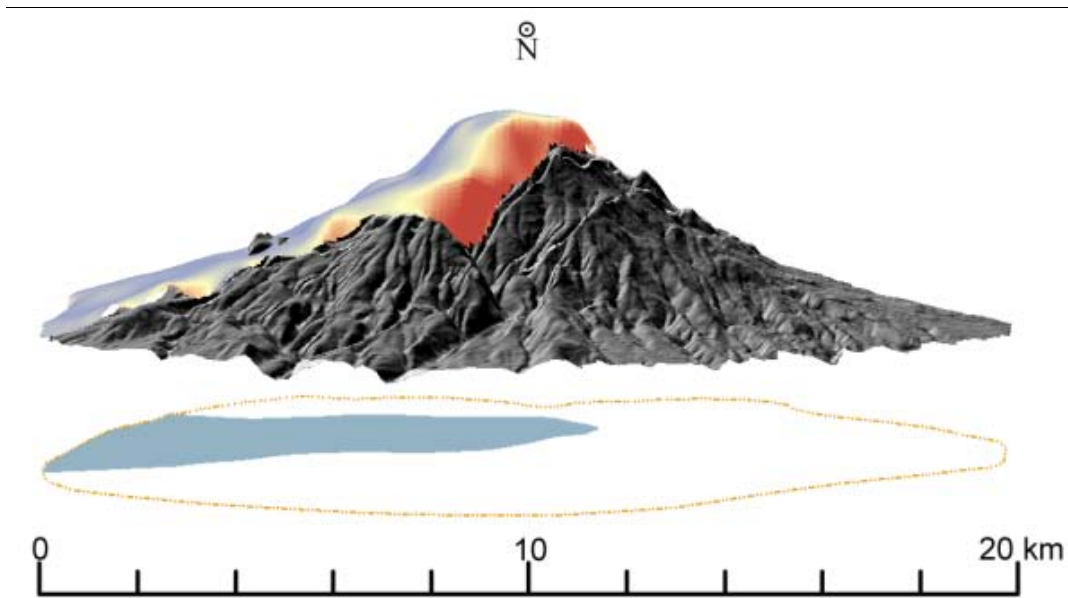


Figure 21 A schematic diagram where the volume of the Barriles deposit is returned to the modern edifice to model pre-collapse conditions. Because of the dominant andesite and its prevalence, the volcano may have accumulated a massive and fairly homogeneous dome of andesite before collapse. The same process was completed for the Caisán Edifice. Note: the modern summit is completely covered and a new elevation of 3.5 km is obtained from the Barriles model; a new elevation of 3.8 km is calculated from the Caisán model.

The polygon defining the edifice, a footprint, clips the 10m DEM as a horizontal slice beginning at the 1,300m contour line (i.e. the point of lowest elevation) and has a plan area of 227 km² (Figure 19). Figure 20 shows the Barú edifice with a clipped flank DEM as a north-to-south 3D cross-section. The horizontal gray shadow underlying the edifice (the footprint) intersects the topography at the 1,300m contour and provides the base height for volume calculations. The entire volume contained in this clipped region is ~150 km³, this includes the flanks, toreva block segments, recent fill from pyroclastic deposits within the crater, and the young dome complex.

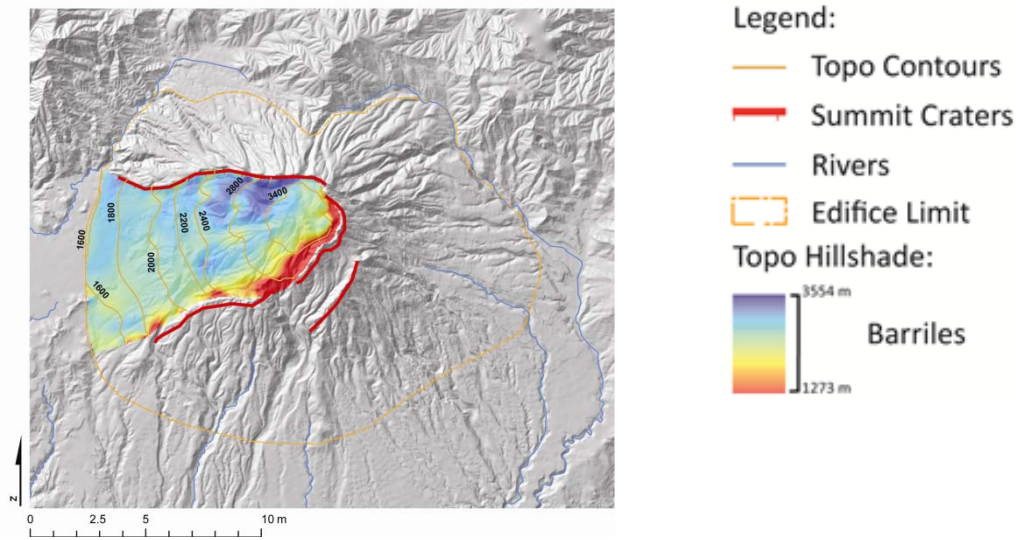


Figure 22 Pre-collapse conditions: Barriles Edifice, the reconstructed edifice. This is a plan view of the hillshade image shown in Figure 21. The same process was completed for the Caisán Edifice.

Volumes determined from the deposit thickness data can be, in theory, added to Volcán Barú’s modern edifice in order to estimate the probable edifice pre-collapse heights. These volumes should not be treated as exact values because precollapse conditions could have varied in a number of ways; it is also realized that debris avalanche deposits increase their volume with dilation and through secondary components they entrain during the emplacement process (Bernard et al., 2008; Bernard et al., 2009; Ownby et al., 2007; van Wyk de Vries et al., 2001; Voight et al., 1983). This study does not have data for estimating “bulking” that may have occurred after the collapse was triggered.

The old edifice must have housed a volume similar to the deposit volumes. Theoretical volume may demand a summit elevation higher than now observed, but it should not violate geomorphological sense. This method attempts to conserve the general edifice slope (determined as 11.75°) and not exceed the footprint size. One edifice that fits conditions for causing the emplacement of the Barriles Deposit is in Figures 21 and 22.

TABLE 8 VOLUME ESTIMATES OF VOLCÁN BARÚ'S VDADS

	Barriles Model	Caisán Model
Edifice Reconstruction (Figure 18)	27 km ³	42 km ³
Voronoi Method (Figure 13)	36 km ³	52 km ³
Isopach Method (Figure 14)	39 km ³	63 km ³
Estimation	30 ±5km ³	50±10 km ³

Volcanic activity since the last collapse accounts for ~10 km³ of dome rock and pyroclastic material found within the amphitheater (Sherrod et al., 2007). After edifice reconstruction, this volume is subtracted before determining the difference between the pre-failure edifice and the current edifice. The values summarized in Table 8 show that edifice reconstruction for both, Barriles and Caisán conditions, provides lower volumes than deposit volumes determined by thickness and area data. This means that pre-collapse elevations for both avalanches may have been significantly higher than the current Barú summit elevation. The “Estimation” values in Table 8 reflect uncertainties based on the three different processes used to calculate sector collapse volumes.

Discussion

Sources and Timing of Events

Volcanic debris avalanche deposits cannot always be traced back to their sources, but the Barriles deposit can be traced (even traversed on foot) back to a gaping, breached crater. The Caisán Deposit, dominantly hidden by material thousands of years younger is not so clearly directed. Based mainly on lithological similarity I argue that Volcán Barú is the source of both of these deposits. Hand specimen mineralogy and texture, especially of the dominant andesite is critical in this conclusion. This rock type represents the Barú dome rock. A comprehensive geochemical study would be required to address this question.

New age dating information for the Barú region is compiled in Table 4. Carbon samples from the two debris avalanche deposits (GPS points 072 and 309) give 8000 ± 30 BP and 8590 ± 50 BP (2 sigma error). These values were averaged to yield a range of 9250-9020 BP. Outcrop exposures of the Barriles Deposit often show a layer of pyroclastic material in sharp contact with the debris avalanche (see photo in Figure 11) but radiocarbon was only sampled from within the VDADs during this study. The dated charcoal samples were completely carbonized and there is evidence in numerous places of pyroclastic material in the VDAD.

Surveys conducted in 2007 by a USAID-supported USGS investigation yielded other radiocarbon dates that constrain the most recent volcanic history of Volcán Barú. Several dates collected from carbon within tephra units found on the north and eastern flanks provided anomalously old values. From samples S07-VB56A and S07-VB98-2, reported to the 2nd sigma, are: 8340 ± 60 BP and 9825 ± 60 BP respectively (Sherrod et al., 2007). These data support the hypothesis that sector collapse occurred during a volcanically active time period.

An additional, older date is from the USGS sample S07-VB98-1. This sample, within pyroclastic deposits on the northern flank yielded 15,450-16,179 BP (Sherrod et al., 2007). This range represents explosive volcanic activity that predates the emplacement of the Barriles Deposit but is too young to represent

TABLE 9 RADIOMETRIC DATE FROM THE BARÚ REGION

#	x	y	Sample ID/Reference	Deposits Dated	Age
1	301673	970533	072	Debris avalanche (Barriles)	8000±30 BP ¹
2	334865	972684	S07-VB56A	Tephra	8340±60 BP ²
3	301601	970332	309	Debris avalanche (Barriles)	8590±50 BP ¹
4	331411	978051	S07-VB98-2	Tephra	9825±60 BP ²
5	331411	978051	S07-VB98-1	Tephra	13,315±80 BP ²
6	300714	960829	065	Debris avalanche (Caisán)	43,350±750 BP ¹
7	326301	936025	248	Debris avalanche (Caisán)	>43,500 BP ¹
8	340254	973213	PAN-06-166	Andesite	0.18±0.08 Ma ³
9	337490	974820	PAN-06-168	Andesite	0.19±0.09 Ma ³
10	324735	940222	PAN-06-136	Andesite	0.32±0.06 Ma ³
11	n/a		IRHE, 1985	Andesite	0.46±0.15 Ma ⁴
12	326350	955330	PAN-06-176	Andesite	0.48±0.08 Ma ³
13	n/a		Sherrod et al. 2007	Andesite: Lava Flows	≤0.78 Ma ⁵

Notes: X and Y coordinates are UTM WGS 84. Radiocarbon from this study¹; Radiocarbon from Sherrod et al. (2007)², ⁴⁰Ar/³⁹Ar dates from Wegner et al. 2011³; K/Ar from IRHE, 1985⁴, and results from several sampled lava flows that were checked for normal polarity from Sherrod et al. (2007)⁵. Radiocarbon results are reported as uncalibrated values radiocarbon years before present (BP) with 2nd sigma errors. Radiometric dates younger than the Barriles emplacement are reported in Table 2.

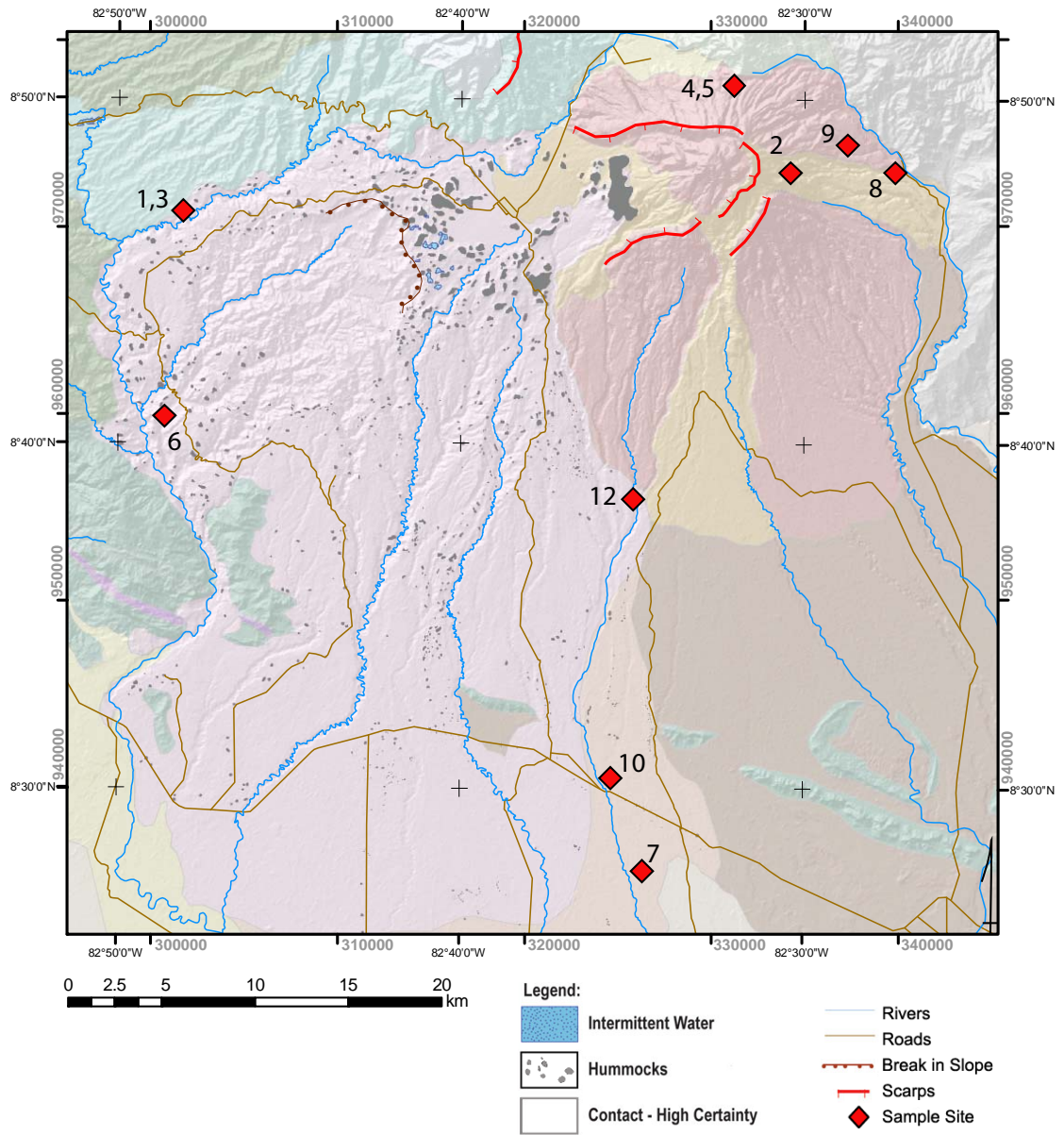


Figure 23 Sites for radiometric samples. All sites from Table 9 are located here except for 11 and 13 as they do not have coordinates.

syneruptive activity that preceded formation of the Caisán Deposit. Two attempted dates from Caisán (Table 1; 248 and 065) are inconclusive with radiocarbon methods. One sample was radiocarbon dead (GPS 248). The

second sample, GPS 065, provided a range of 48,636 – 45,224 BP, at the edge of credible 14C.

$^{40}\text{Ar}/^{39}\text{Ar}$ dates were recently reported in a paper focusing on the general magmatic history of the Central American landbridge by Wegner et al. (2011). The dates shown in Table 9 represent the values that are important to Volcán Barú's edifice collapse. GPS locations provided for the samples pinpoint them within areas where lava, debris flows, block and ash, and potentially VDADs are outcropping. Just north of the Interamerican HWY, sample PAN-06-136 (0.32 Ma) was likely collected from the steep scarp of the Río Piedra below the HWY bridge; this could be dating material from the Caisán Deposit or potentially from interbedded lahar units. Located at the headwaters of Río Piedra, PAN-06-176 (0.48 Ma) was collected near sites I visited where avalanche deposits are exposed but there are also overlying block and ash units that could have been sampled within the deep river scarps. The samples PAN-06-168 and PAN-06-166 are taken from the eastern flank. "168" (0.19 Ma) comes from an area that Rausch (2007) described as debris flows from the flank while "166" (0.18 Ma, the youngest date listed) likely comes from the massive outcrop of entablature andesite, a truncated lava flow in the area of Horqueta.

Radiometric dating of lavas associated with Volcán Barú reveal an active history that began less than 0.5 million years ago. Lava flows that were sampled during the USGS investigation from 2007 had normal polarity and this result is consistent with no sample being older than 0.78 Ma (Sherrod et al., 2007). These dates are several hundred thousand years younger than the neighboring volcanic complex, Tisingal, where the ages range from 0.92-1.66 Ma (UTP, 1992).

Hummock Data Comparisons

Hummocks can travel tens of kilometers and survive the emplacement process and millennia of weathering as >5m high hills. Fragile material and characteristics such as entrained soil and wood fragments, original stratigraphy, and high topographic relief are still visible despite Panama's warm, tropical environment. Digitized hummock maps were used to compare hummock distributions at Barú and Mount St. Helens (Glicken, 1986), Mount Shasta (Crandall, 1989), Parinacota (ref), Las Isletas and El Crater Deposits from

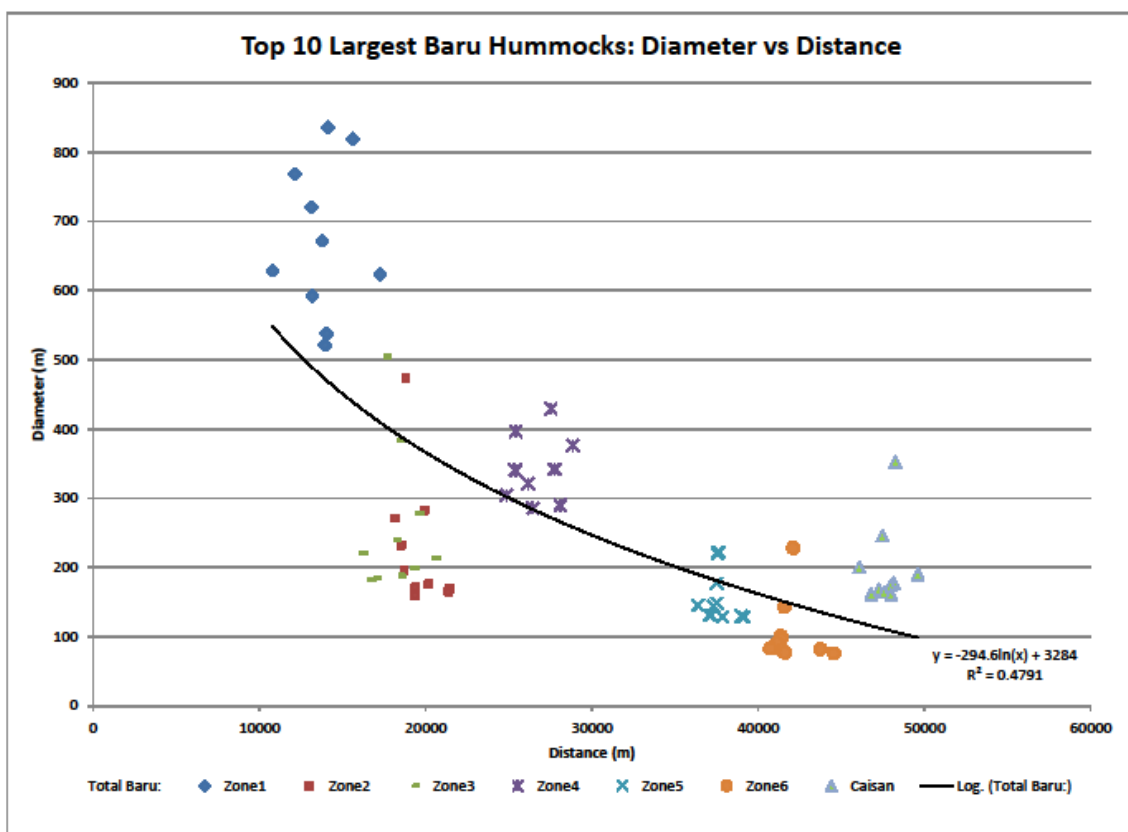


Figure 24 The 10 largest hummock diameters for each zone of Barú's deposits are plotted. The relationship between distance and maximum hummock diameter shows anomalously large diameters for Zone 4 hummocks, perhaps reflecting effects of topographic irregularities (see text for details)

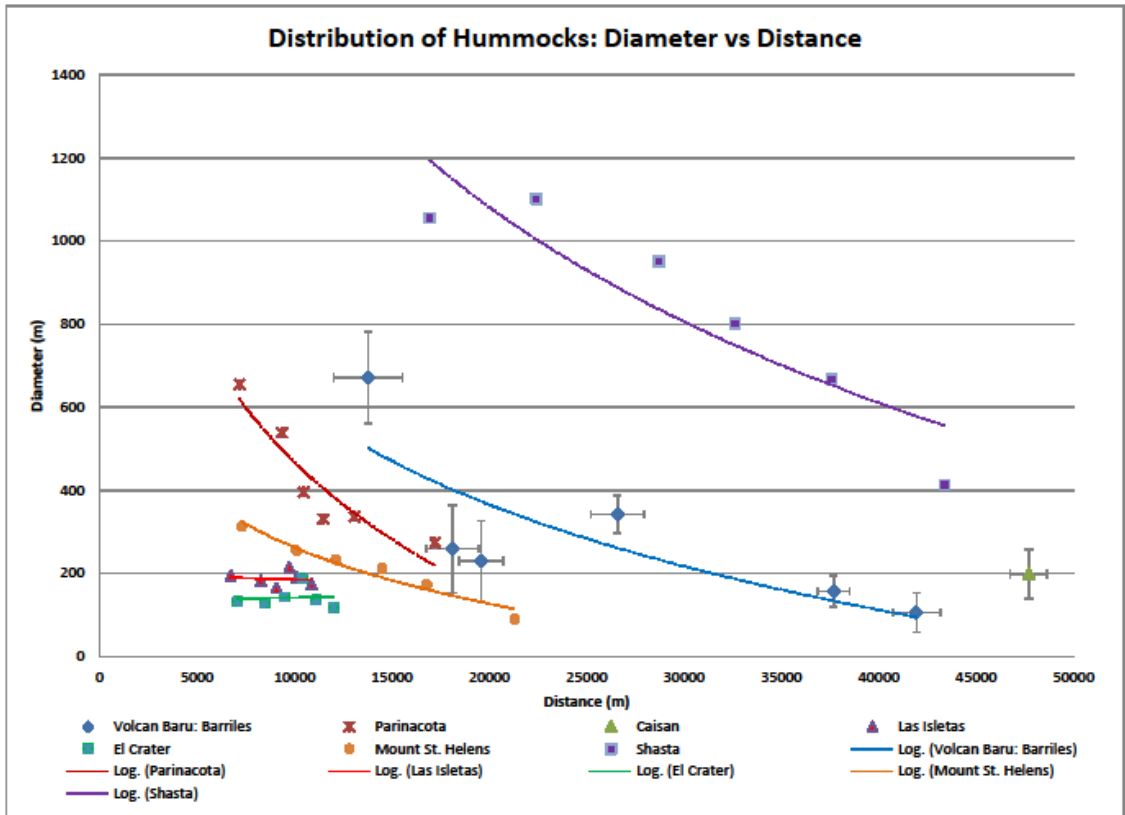


Figure 25 Hummock diameter/distance relationships in various debris avalanche deposits: Volcán Barú: Barriles and Caisán, Parinacota, Mombacho: El Crater and Las Isletas, Mount Shasta, and Mount St. Helens

Mombacho (Shea and Van Wyk deVries, 2008). Hummock GPS data was directly available from Glicken’s work and was determined from maps for the other sources.

Hummock diameters generally decrease with distance (Figure 25). This trend is not obvious for small VDADs such as those from Mombacho, but is very clear in larger deposits.

VDAD Mobility

Table 10 compares the dimensions of VDADs, showing deposits from Volcán Barú represent the largest subaerial deposits so far known. The estimated volumes range from 27 to 39 km³ and 42 to 63 km³ for Barriles and Caisán Deposits respectively; allowing for error these values are reported as 30±5 km³ and 50±10 km³. Figure 26 plots the relationship between source height and distance travelled and Figure 27 the area/volume relationships. On both plots the position of Barú deposits plot near the high-volume examples such as Mount Shasta.

TABLE 10 (NEXT PAGE) EXAMPLES OF SUBAERIAL VDADS

Note: “0” values indicate no calculations have been made. Length of runout “L,” drop height “H,” mobility calculation “H/L,” calculated volume “V” are listed here with the primary sources of information for reference. Sources are tabulated with the corresponding data. *Indicates theoretical values from this study.

Name	Country	Source	L (km)	H (km)	H/L	V (km ³)	Area (km ²)
Acatenango	Guatemala	Siebert, 2006	42	3.78	0.09	5	210
Akagi	Japan	Siebert, 1984	19	2.4	0.13	4	0
Asama	Japan	Siebert, 1984	20	2.25	0.11	2	0
Avachinsky	Russia	Ponomareva, 2006	30	3	0.10	18	300
Bandai	Japan	Siebert, 1984	11	1.2	0.11	1.5	34
Barú: Barriles	Panama	this study	45	3.5*	0.08	30	966
Barú: Caisán	Panama	this study	51	3.8*	0.07	50	1162
Bezymianny	Russia	Gorshkov and Dubik, 1970	18	2.4	0.13	1.5	500
Chimborazo	Ecuador	Bernard, 2008	35	6.2	0.17	11	280
Colima	Mexico	Siebert, 1984	40	4	0.10	10	900
Egmont 1	New Zealand	Siebert, 1984	31	2.6	0.08	7.5	250
Egmont 2	New Zealand	Siebert, 1984	21	2.4	0.11	1	0
Fuego/Acat.	Guatemala	Siebert, 2006	50	4	0.08	15	440
Galunggung	Indonesia	Siebert, 2002	23	1.9	0.08	16	170
Iizuna	Japan	Siebert, 2002	17	0.8	0.13	5	0
Irazu	Costa Rica	Siebert, 2006	13	1.82	0.14	1.5	35
Iriga	Philippines	Siebert, 1984	11	1.05	0.10	1.5	65
Jocotitlán	Mexico	Siebe, 1992	12	1.32	0.11	2.8	80
Mawenzi	Tanzania	Hayashi and Self, 1992	60	4.5	0.08	7.1	1150
Meru	Tanzania	Siebert, 2002	50	3.9	0.08	15	1400
Miravalles	Costa Rica	Siebert, 2006	19	2.09	0.11	7	110
Mombacho: EC	Nicaragua	Shea, 2008	12	1.5	0.12	1.8	51
Mombacho: LI	Nicaragua	Shea, 2008	11	1.345	0.11	1.2	55
Mount St. Helens	USA	Glicken, 1996	22	2.949	0.12	2.6	64
Pacaya	Guatemala	Siebert, 2006	25	2.5	0.10	1	55
Parinacota	Chile	Clavero, 2002	21	2	0.30	6	140
San Vicente	El Salvador	Siebert, 2006	24	2.16	0.09	1	0
Santa Ana	El Salvador	Siebert, 2006	48	1.92	0.04	16	540
Shasta	USA	Crandell, 1989	57	4.3	0.08	45	571
Shiveluch: "Old"	Russia	Belousov, 1999	35	4	0.11	31.5	350
Shiveluch: 1964	Russia	Belousov, 1999	16	2.3	0.14	1.5	98
Socompa	Ecuador	Wadge, 1995	35	3.3	0.09	36	490
Tacaná	Guatemala	Siebert, 2006	8	2.8	0.35	1	6
Tancitaro	Mexico	Morelli, 2010	73	3.55	0.04	18	1155
Taunshits	Russia	Siebert, 1984	17	1.2	0.07	1	0
Tecuamburro	Guatemala	Siebert, 2006	15	1.8	0.12	4	0
Tenorio	Costa Rica	Siebert, 2006	17	2	0.70	2	100
Turrialba	Costa Rica	Siebert, 2006	15	1.05	0.07	1	21.5
Yatsugatake	Japan	Siebert, 1984	50	2.6	0.05	10	0
Zempoala	Mexico	Arce, 2008	80	2.79	0.03	6	600

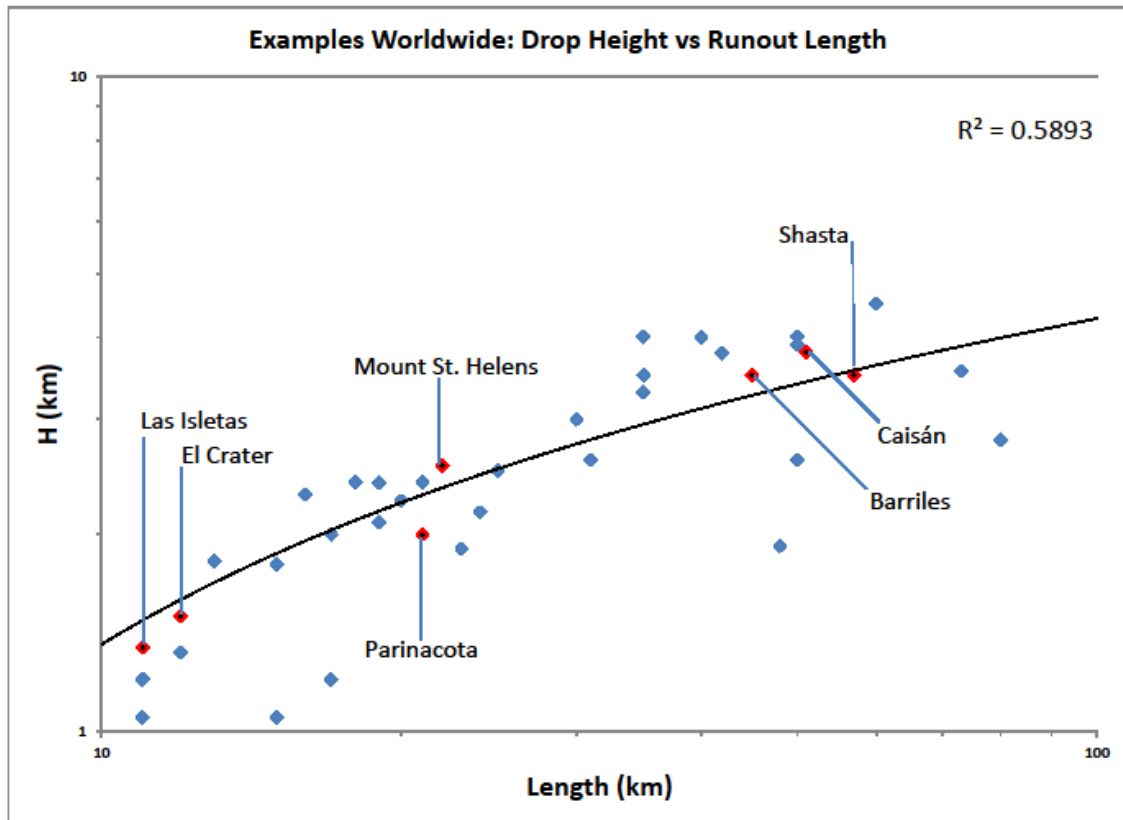


Figure 26 Relative drop height vs. horizontal distance of 40 VDAD deposits; (point data listed in Table 10). Best-fit trend line is a logarithmic regression (R^2 value of 0.5893); [equation $y = 1.2659\ln(x) - 1.5579$].

Debris avalanches from Volcán Barú (H/L of 0.08 and 0.07; Table 10) are relatively mobile and similar to Mount Shasta, USA (0.089) and Socompa, Chile/Argentina (0.94).

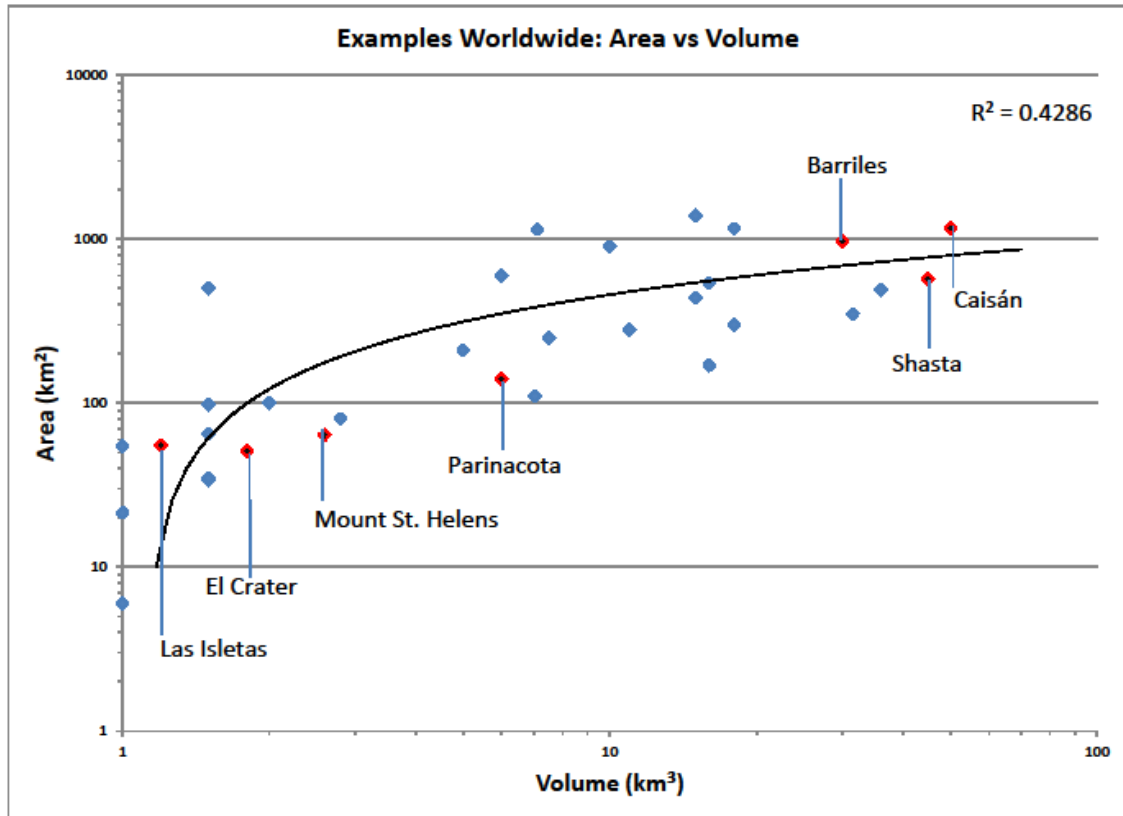


Figure 27 Deposit area and volume relationship based on examples from 40 VDADs; see Table 10. Data is plotted on a log scale; a log trend is used to represent the general increase of Area with Volume; $[y = 209.03\ln(x) - 23.459]$. The R^2 value is 0.4286 suggesting scatter in the data.

Conclusions

Volcán Barú has produced two major debris avalanches. Each of these deposits is mainly composed of andesitic material that likely represents collapse of an active volcanic summit that removed a significant dome complex; a 58° sector (10x6 km) is missing from the edifice. The scale of the domes was impressive and the volume of debris avalanche material is large based on comparisons with other volcanoes around the world. Weakening process likely included intense hydrothermal alteration within the edifice as well as concurrent dome growth. Trigger mechanisms were likely related to active volcanism

(explosive activity, dike intrusion, or cryptodome conditions) although other short timescale events are also candidates (earthquake or hydrologic events). Emplacement mechanisms relied on lateral extension of the massive debris avalanche that resulted in toreva block formation, internal shearing, widespread transport of blocks and hummocks, and sufficient basal friction to entrain secondary material from basement rock.

The date of the older collapse is not well constrained, but it is possible that Barú has emplaced and collapsed major volumes ($>30 \text{ km}^3$) of andesite domes twice in the past 50,000 years. This makes Barú a hazardous volcano worth monitoring, as work by Sherrod et al. 2007 has already indicated. The geometry and volume of the current dome suggests that the same kind of collapse could eventually occur again if volumes increase and a triggering mechanism such as explosive volcanism occurs.

References

- Adames, A., 1988, Panama Universities: Estudios Sociales Centroamericanos, p. 7-16.
- AdGeo, 2008, Informe Ingeniero--Geológico de Prefactibilidad; Proyecto Hidroeléctrico Pedregalito: Provincia de Chirquí, Generadora Pedregalito, S.A.: Panama, Empresa Advanced Geology Consultants, S.A., p. 222.
- Alverson, W.S., 1989, *Matisia-Exalata* (Bombacaceae), a New Species from the Highlands of Central Panama: *Systematic Botany*, v. 14, p. 473-475.
- Anchukaitis, K.J., and Horn, S.P., 2005, A 2000-year reconstruction of forest disturbance from southern Pacific Costa Rica: *Palaeogeography Palaeoclimatology Palaeoecology*, v. 221, p. 35-54.
- Behling, H., 2000, A 2860-year high-resolution pollen and charcoal record from the Cordillera de Talamanca in Panama: a history of human and volcanic forest disturbance: *Holocene*, v. 10, p. 387-393.
- Belousov, A., Belousova, M., and Voight, B., 1999, Multiple edifice failures, debris avalanches and associated eruptions in the Holocene history of Shiveluch volcano, Kamchatka, Russia: *Bulletin of Volcanology*, v. 61, p. 324-342.
- Belousov, A.B., 1995, The Shiveluch volcanic eruption of 12 November 1964: Explosive eruption provoked by failure of the edifice, in Ida, Y., and Voight, B., eds., *Models of magmatic processes and volcanic eruptions*, Volume 66, *Journal of Volcanology and Geothermal Research*, p. 357-365.
- Benjamín, A.T., 2004, *En Panamá sí tiembla*, La Prensa Web: Ciudad de Panama, La Prensa.
- Bernard, B., de Vries, B.V., Barba, D., Leyrit, H., Robin, C., Alcaraz, S., and Samaniego, P., 2008, The Chimborazo sector collapse and debris avalanche: Deposit characteristics as evidence of emplacement mechanisms: *Journal of Volcanology and Geothermal Research*, v. 176, p. 36-43.
- Bernard, B., van Wyk de Vries, B., and Leyrit, H., 2009, Distinguishing volcanic debris avalanche deposits from their reworked products: the Perrier sequence (French Massif Central): *Bulletin of Volcanology*, v. 71, p. 1041-1056.
- Buchs, D.M., Baumgartner, P.O., Baumgartner-Mora, C., Bandini, A.N., Jackett, S.J., Diserens, M.O., and Stucki, J., 2009, Late Cretaceous to Miocene seamount accretion and melange formation in the Osa and Burica peninsulas (Southern

- Costa Rica): episodic growth of a convergent margin, in James, K.H., Lorente, M.A., and Pindell, J.L., eds., *The Origin and Evolution of the Caribbean Plate*, GSL Special Publication 328, p. 411–456.
- Camacho, E.A., 1998, *Los Volcanes en Panama*, in Panama, U.d., ed., Instituto de Geociencias, Universidad de Panama, Volume 2007: Ciudad de Panama, Panama, Universidad de Panama, Instituto de Geociencias.
- Camacho, E.A., and Benito, B., 2008, *Evaluación de la Amenaza Sísmica en Panamá, RESIS II*, Instituto de Geociencias Universidad de Panamá & Universidad Politécnica de Madrid, p. 161.
- Carr, M.J., Feigenson, M.D., Patino, L.C., and Walker, J.A., 2003, *Volcanism and geochemistry in Central America: Progress and problems*, in Eiler, J.M., ed., *Inside the Subduction Factory*, Volume 138, AGU Geophysical Monograph Series, p. 153–174.
- Carr, M.J., Patino, L.C., and Feigenson, M.D., 2007, *Petrology and Geochemistry of Lavas*, in Bundschuh, J., and Alvarado, G., eds., *Central America: Geology, Resources and Hazards*, Volume 1: London, Taylor & Francis, p. 201-237.
- Chang, K., 2006, *Introduction to Geographic Information Systems*: New York, McGraw-Hill, 432 p.
- Clement, R.M., and Horn, S.P., 2001, *Pre-Columbian land-use history in Costa Rica: a 3000-year record of forest clearance, agriculture and fires from Laguna Zoncho: Holocene*, v. 11, p. 419-426.
- Coates, A.G., Jackson, J.B.C., Collins, L.S., Cronin, T.M., Dowsett, H.J., Bybell, L.M., Jung, P., and Obando, J.A., 1992, *Closure of the Isthmus of Panama - the near-Shore Marine Record of Costa-Rica and Western Panama: Geological Society of America Bulletin*, v. 104, p. 814-828.
- Crandell, D.R., Miller, C.D., Glicken, H.X., Christiansen, R.L., and Newhall, C.G., 1984, *Catastrophic Debris Avalanche from Ancestral Mount Shasta Volcano, California: Geology*, v. 12, p. 143-146.
- de Boer, J.Z., M.S., D., Bordelon, M.J., Defant, M.J., Bellon, H., and Maury, R.C., 1995, *Cenozoic magmatic phases of the Costa Rican island arc (Cordillera de Talamanca)*, in Mann, P., ed., *Geologic and Tectonic Development of the*

- Caribbean Plate Boundary in Southern Central America, Volume 295: Boulder, Geological Society of America, p. 35-55.
- Defant, M.J., Jackson, T.E., Drummond, M.S., Deboer, J.Z., Bellon, H., Feigenson, M.D., Maury, R.C., and Stewart, R.H., 1992, The Geochemistry of Young Volcanism Throughout Western Panama and Southeastern Costa-Rica - an Overview: *Journal of the Geological Society*, v. 149, p. 569-579.
- Glicken, H., 1986, Rockslide-debris avalanche of May 18, 1980, Mount St. Helens Volcano, Washington [Doctoral thesis]: Santa Barbara, University of California Santa Barbara.
- Glicken, H., 1991, Sedimentary architecture of large volcanic-debris avalanches, in Fisher, R.V., and Smith, G.A., eds., *Sedimentation in Volcanic Settings*, SEPM Spec. Publ., p. 99-106.
- Glicken, H., 1996, Rockslide-debris avalanche on May 18, 1980, Mount St. Helens Volcano, Washington, Open-File Report 96-677: Reston, VA, The U.S. Geological Survey, p. 98.
- Griggs, R.F., 1920, The great Mageik landslide: *Ohio Journal of Science*, v. 20, p. 325-354.
- Hackett, W.R., and Houghton, B.F., 1989, A Facies Model for a Quaternary Andesitic Composite-Volcano - Ruapehu, New-Zealand: *Bulletin of Volcanology*, v. 51, p. 51-68.
- Hidalgo, P., Vogel, T.A., Currier, R., Layer, P., and Rooney, T., 2009, The Origin of El Hato Silicic Ignimbrite of El Valle Volcano, Panama: Evidence of Deep Fractionation Processes: *Geological Society of America Abstracts with Programs*, v. 41, p. 353.
- Knutsen, K.L., 2010, La Yeguada Volcanic Complex, Western Panama: An Assessment of the Geologic Hazards Using New $^{40}\text{Ar}/^{39}\text{Ar}$ Ages [Masters thesis]: Houghton, Michigan Tech University.
- Linares, O.F., Sheets, P.D., and Rosenthal, E.J., 1975, Prehistoric Agriculture in Tropical Highlands: *Science*, v. 187, p. 137-145.
- Lockwood, J.P., and Hazlett, R.W., 2010, *Volcanoes : Global Perspectives*: Hoboken, NJ, Wiley-Blackwell, ix, p.539.

- Major, J.J., and Iverson, R.M., 1999, Debris-flow deposition: Effects of pore-fluid pressure and friction concentrated at flow margins: *Geological Society of America Bulletin*, v. 111, p. 1424-1434.
- Mann, P., Rogers, R.D., and Gahagan, L., 2007, Overview of plate tectonic history and its unresolved tectonic problems, in Bundschuh, J., and Alvarado, G., eds., *Central America: Geology, Resources and Hazards, Volume 1*: London, Taylor & Francis, p. 1974.
- Minerales, D.G.d.R., 1976, Mapa Geológico: República de Panamá: Panamá, Instituto Geográfico Nacional "Tommy Guardia" (IGNTG), p. Map col. map 36 x 66 cm.
- Minerales, D.G.d.R., 1991, Mapa Geológico: República de Panamá: Panamá, Instituto Geográfico Nacional "Tommy Guardia," (IGNTG).
- Montessus de Ballore, F., comte de, 1884, *Temblores y erupciones volcánicas in Centro-América, con un apéndice meteorológico*: San Salvador, F. Sagrini.
- Morell, K.D., Fisher, D.M., and Gardner, T.W., 2008, Inner forearc response to subduction of the Panama Fracture Zone, southern Central America: *Earth and Planetary Science Letters*, v. 265, p. 82-95.
- Morelli, S., Monroy, V.H.G., Gigli, G., Falorni, G., Rocha, E.A., and Casagli, N., 2010, The Tancitaro Debris Avalanche: Characterization, propagation and modeling: *Journal of Volcanology and Geothermal Research*, v. 193, p. 93-105.
- Neumann van Padang, M., 1939, Über die vielen tausend Hügel in westlichen Vorlande des Raoeng-Vulkans (Ostjava): *De ingenieur in Nederlandsch-Indië*, v. 6, p. 35-41.
- Ownby, S., Granados, H.D., Lange, R.A., and Hall, C.M., 2007, Volcan Tancitaro, Michoacan, Mexico, $40\text{Ar}/39\text{Ar}$ constraints on its history of sector collapse: *Journal of Volcanology and Geothermal Research*, v. 161, p. 1-14.
- Palmer, B.A., Alloway, B.V., and Neall, V.E., 1991, Volcanic-debris avalanche deposits in New Zealand—Lithofacies organization in unconfined, wet-avalanche flows, in Fisher, R.V., and Smith, G.A., eds., *Sedimentation in Volcanic Settings, Volume 45*, SEPM Special Publication, p. 89–98.
- Ponomareva, V.V., Melekestsev, I.V., and Dirksen, O.V., 2006, Sector collapses and large landslides on Late Pleistocene–Holocene volcanoes in Kamchatka, Russia: *Journal of Volcanology and Geothermal Research*, v. 158, p. 117-138.

- Reiche, P., 1937, The Toreva-block, a distinctive landslide type: *The Journal of Geology*, v. 45, p. 538-548.
- Restrepo, J.F., 1987, A geochemical investigation of Pleistocene to recent calc-alkaline volcanism in western Panama [Masters thesis]: Tampa, University of South Florida.
- Sekiya, S., and Kikuchi, Y., 1889, The eruption of Bandai-san: *Tokyo Imp. Univ. Coll. Sci. J.*, v. 3, p. 91-172.
- Shea, T., de Vries, B.V., and Pilato, M., 2008, Emplacement mechanisms of contrasting debris avalanches at Volcan Mombacho (Nicaragua), provided by structural and facies analysis: *Bulletin of Volcanology*, v. 70, p. 899-921.
- Sherrod, D.R., Vallance, J.W., Tapia Espinosa, A., and McGeehin, J.P., 2007, Volcán Barú eruptive history and volcano-hazards assessment, Open-File Report 2007-1401: Reston, VA, The U.S. Geological Survey, p. 33.
- Siebert, L., 1984, Large volcanic debris avalanches: Characteristics of source areas, deposits, and associated eruptions: *Journal of Volcanology and Geothermal Research*, v. 22, p. 163-197.
- Siebert, L., 1996, Hazards of large volcanic debris avalanches and associated eruptive phenomena, in Scarpa, R., and Tilling, R.I., eds., *Monitoring and mitigation of volcano hazards*: Berlin, Springer-Verlag, p. 541-572.
- Siebert, L., Kimberly, P., Calvin, C., Luhr, J., and Mattiotti, G.K., 2006, *Smithsonian Global Volcanism Program: Volcanoes of Mexico and Central America*, Digital Information Series, GVP-7, CD-ROM.
- Siebert, L., and Simkin, T., 2002-, *Volcanoes of the World: an Illustrated Catalog of Holocene Volcanoes and their Eruptions*, Global Volcanism Program Digital Information Series, Volume GVP-3, Smithsonian Institution.
- Tibaldi, A., 2001, Multiple sector collapses at Stromboli volcano, Italy: how they work: *Bulletin of Volcanology*, v. 63, p. 112–125.
- Tucker, M.E., 1996, *Sedimentary rocks in the field*: Chichester, West Sussex, England; New York, Wiley, viii, p. 153.
- Ui, T., 1983, Volcanic Dry Avalanche Deposits - Identification and Comparison with Nonvolcanic Debris Stream Deposits: *Journal of Volcanology and Geothermal Research*, v. 18, p. 135-150.

- Ui, T., Glicken, H., 1986, Internal structural characteristics of a debris avalanche from Mount Shasta, California, U.S.A.: *Bulletin of Volcanology*, v. 48, p. 189-194.
- Ui, T., Kawachi, S., and Neall, V.E., 1986, Fragmentation of Debris Avalanche Material during Flowage - Evidence from the Pungarehu Formation, Mount Egmont, New-Zealand: *Journal of Volcanology and Geothermal Research*, v. 27, p. 255-264.
- Ui, T., Takarada, S., and Yoshimoto, M., 2000, Debris Avalanches, in Sigurdsson, H., ed., *Encyclopedia of Volcanoes*: San Diego, California, Academic Press, p. 617-626.
- USGS, 2008, USGS and USAID Announce U.S.-Panamanian Action in Response to a Joint Study of Panama's Baru Volcano: englishnews-panama.com, English News Panama.
- UTP, 1992, Evaluación de la amenaza, estimación de la vulnerabilidad y del factor costo del riesgo del Volcán Barú, Republica de Panamá: Panama, Departamento de Geotécnica Facultad de Ingeniería Civil, Universidad Tecnológica de Panamá, p. 129.
- van Wyk de Vries, B., Self, S., Francis, P.W., and Keszthelyi, L., 2001, A gravitational spreading origin for the Socompa debris avalanche: *Journal of Volcanology and Geothermal Research*, v. 105, p. 225-247.
- Voight, B., Janda, R.J., Glicken, H., and Douglass, P.M., 1983, Nature and Mechanics of the Mount St-Helens Rockslide-Avalanche of 18 May 1980: *Geotechnique*, v. 33, p. 243-273.
- Wadge, G., Francis, P.W., and Ramirez, C.F., 1995, The Socompa Collapse and Avalanche Event: *Journal of Volcanology and Geothermal Research*, v. 66, p. 309-336.
- Wegner, W., Wörner, G., Harmon, R.S., and Jicha, B.R., 2011, Magmatic history and evolution of the Central American Land Bridge in Panama since Cretaceous times: *Geological Society of America Bulletin*, v. 123, p. 703-724.
- Williams, H., 1941, Calderas and their origin: *California University Publications in Geological Sciences*, v. 25, p. 239-346.

Appendix

Location Map

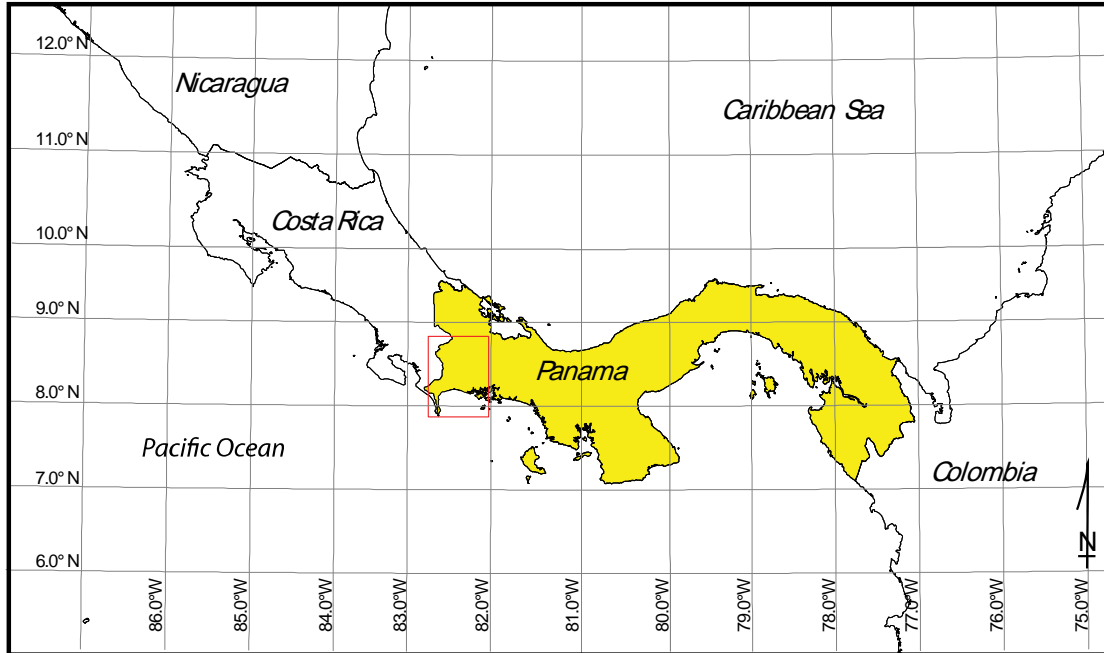


Figure 28 Location map of Panama with the site area captured in the red rectangle (center of view).

Deposit Mineralogy

TABLE 11 MINERALOGY OF SAMPLES: BARRILES AND CAISÁN DEPOSITS

Barriles	GPS ID	hnblld	plag	qtz	pyx	xenoliths*	vesicles	Facies
1	309	10	15	0	2	2	2	Block
2	286	5	5	0	3	1	15	Block
3	287	1	1	0	2	0	15	Block
4	282	3	3	0	2	0	0	Block
5	248	2	5	1	5	1	15	Mixed
6	205A	0	1	0	5	0	2	Block
7	205B	0	5	0	15	0	2	Block
8	193	1	3	0	2	0	2	Block
9	179	3	3	0	1	1	0	Mixed
10	049	2	1	1	3	0	5	Block
11	047	2	5	0	15	0	0	Block
12	028	1	1	0	3	0	0	Block
13	022	0	0	0	7	1	10	Block
14	190	3	5	0	15	0	0	Block
Caisán	GPS ID	hnblld	plag	qtz	pyx	xenoliths*	vesicles	Facies
1	301	5	7	2	3	3	2	Mixed
2	298	3	1	3	0	0	0	Mixed
3	293	5	2	0	3	0	15	Mixed
4	291	3	5	1	0	1	5	Mixed
5	274	1	1	1	0	0	5	Mixed
6	248	2	5	1	5	3	1	Mixed
7	246	1	1	1	5	0	15	Block
8	202	0	3	0	15	0	3	Block
9	168	1	1	0	2	0	0	Block
10	164	1	3	0	2	0	0	Block
11	163	7	20	0	1	0	5	Block
12	065	3	15	0	0	0	5	Block

* Xenoliths are listed as quantity identified instead of percentage.

Regional Geology

Figure 29 Geologic descriptions for units identified during this study as well as compiled information from current literature. Sources are summarized in Table 1. Holocene

- Hc** Fluvial deposits from the Río Chiriquí Viejo drainage; continental sediments dominated by well-sorted sand and round gravel-to-cobble clasts of reworked volcanoclastic material and bedrock. Deposits overlie the volcanic debris avalanche deposits (VDADs) from Volcán Barú and spread south to reach the Pacific Ocean (*this study*). Lake sediments are included in this group found on the valley floor of Cerro Punta (*Stewart, 1978*) and among the Barriles hummocks (*personal communication, Ángel Rodríguez*).
- Hal** Alluvial Deposits: Undifferentiated Alluvium dominating the coastal plain reaching the Pacific Ocean east of Panama's shared boundary with Costa Rica. (*French and Schenk, 2004*)
- Hbp** Pyroclastic flows from Volcán Barú; includes tephra, block-and-ash, and volcanoclastics on the flanks and in the proximal, low-lying areas. Fine tephra units have extended from the crater west and southwest but are not represented here; tephra has been found as far west as Laguna Zoncho and Laguna Santa Elena in Costa Rica (*Anchukaitis and Horn, 2005; Clement and Horn, 2001*). Radiocarbon dating from these deposits are as young as 316 calendar years before present (*Sherrod et al., 2007*).
- Hbd** Volcán Barú dome complex; three distinct domes of hornblende-rich andesite, SiO₂ 52-63 wt% (*Rausch, 2007; Sherrod et al., 2007*). This unit is constrained by the 6x10 km, breached summit crater (*Sherrod et al., 2007; Siebert, 2004; this study*).
- Hvda_BD** Barriles Deposit, Volcán Barú volcanic debris avalanche deposits; Total Area: 982 sq km; maximum extent N-S: 45 km; Maximum extent E-W: 28 km.
Hummocks - >3,000 individual hummocks; Height range: 3-97m
Deposit thickness: 1.0-188m
Radiocarbon Date: 8764 & 9490 calendar years before present (95.4% probability)
An agglomeritic deposit with a block and mixed facies. The dominant lithology is subround-subangular, fine-grained, glassy, plag-phyric, hornblende-rich andesite. Contains rip-up clasts of well-sorted fluvium; exotics from the basement limestone and schist, andesitic jigsaw-fractured blocks; a significant amount of hydrothermally altered clasts; and a mottled, very fine matrix. This deposit is often the modern surface with overlying tephra deposits proximal to Volcán Barú's edifice.

Pleistocene

- Pvda_CD** Caisán Deposit, Volcán Barú volcanic debris avalanche deposits; Total Area: 1190 sq km; maximum extent N-S: 51 km; Maximum extent E-W: 28 km.
Hummocks - >1,000 individual hummocks; Height range: 3-10m
Deposit thickness: 3.0-119.8m
Radiocarbon Date: 45,224 calendar years before present (95.4% probability)
An agglomeritic deposit with block and mixed facies. The dominant lithology is subangular, fine-grained, glassy, plag-phyric, hornblende-rich andesite. They contain rip-up clasts of well-sorted fluvium; exotics from the basement limestone and schist, andesitic jigsaw-fractured blocks; a significant amount of hydrothermally altered clasts; and a mottled, very fine matrix. This deposit is often located below 0.2 to 3.0 m of sediment and thin tephra units; outcrop exposures demonstrate this unit is stratigraphically older than the Barriles Deposit.
- Pbl** Volcanoclastics from Volcán Barú; undifferentiated lahar units with interbedded pyroclastic flows. Without direct observation, age relationships could not be determined, but proximity and degree of induration suggest these deposits are older than the volcanic debris avalanche deposits.
- Pbe** Volcán Barú Edifice – K-Ar dating: 0.46Ma +/- 0.15 (*IRHE, 1984*). Undifferentiated andesitic lavas hornblende-rich: SiO₂ 52-63 wt%) and associated pyroclastics interrupted by a major breach in the structure opening to the west. The southern contact is poorly defined due to overlapping lahar and pyroclastic flow units of Qbl. (*Restrepo, 1987; Siebert et al., 2004*)

Quaternary

Qtd Tisingal Dome Complex; andesitic lavas (hornblende-rich: SiO₂ 52-62 wt%) (*Restrepo, 1987*). Radiometric dating: 1.6-0.9Ma (*Universidad Tecnológica de Panama, 1992*).

Quv Undifferentiated Volcanics – From Tisingal and potentially from Volcán Barú. Block and ash flows, pyroclastic flows, volcanoclastics, and tephra. Constrained to the northern boundary of the Río Chiriquí Viejo; the northern contact is poorly defined. (*Stewart, 1978; this study*)

Qte Tisingal Edifice; hornblende-rich andesitic lavas and domes (*Stewart, 1978; Restrepo, 1987*). Radiometric dating: 1.6-0.9Ma (*Universidad Tecnológica de Panama, 1992*).

Tertiary

Tpr Paso Real Lahars (Pliocene): Up to 900m thick; Lahars, breccias, and andesitic lava flows (*Morell et al., 2008*) from the Cordillera de Talamanca 4.3 to 1.2 Ma (*de Boer et al., 1995*); found in the extreme north-western section of this study area.

Tca Charco Azul Group (Late Pliocene)
Subunits:
1. Armuelles Formation – Pliocene-to-Pleistocene; Up to 370m thick; shallow marine sediments with pebbly conglomerates of unconsolidated greenish-blue siltstone; and litharenite with rare beds rich in oyster shells and corals.
2. Burica Formation – Late Pliocene; Up to 2,800m thick; dominantly fine-grained volcanoclastic turbidite sediments with associated megabreccias; contains the “La Chancha Member” (2-4m thick; auto-brecciated unit that overlies 1-2m of basal, coarse volcanic conglomerate).
3. Peñita Formation – Early Pliocene; Up to 1,200m thick but laterally variable; shallow marine clay sediments and turbidites. The base is coarse, greenish-blue litharenite with locally channeled basal volcanic conglomerate. Also contains the La Vaca Member” (up to 900m thick; dominated by coarse, grayish-green volcanic conglomerate with large-scale crossbeds; channels, armored mud balls, and locally, large thick-shelled oysters, other bivalves, and wood.)
4. Cenozoic Seamount Complex – restricted to the western shore of the Burica Peninsula. (*Coates et al., 1992; Buchs et al., 2009*)

Tt Térraba-Curré Formations (Oligocene-Miocene): Up to 2km thick with an associated, unnamed marine mudstone only visible in the central and northwest portions of the Fila Costeña Thrust Belt; conformably overlies the (*Morell et al., 2008*).
Subunits:
1. Térraba Formation – Oligocene-Miocene; is a bioclastic/volcanoclastic turbidite sequence composed primarily of interbedded mudstone and volcanoclastic sandstone with minor black shales, marls and conglomerates (*Morell et al., 2008*). Rare intrusions of 15-11 Ma gabbros (*de Boer et al., 1995*).
2. Curré Formation – Miocene; is a thin, coarsening upwards volcanoclastic sandstone and conglomerate (*Morell et al., 2008*).

Tb Brito Formation – Eocene; up to 1km thick; associated with the thrust faults within the Fila Costeña Thrust Belt region; Bioclastic limestone and turbidite sequence (*Morell et al., 2008*) with rare intrusions of 15-11 Ma gabbros (*de Boer et al., 1995*).

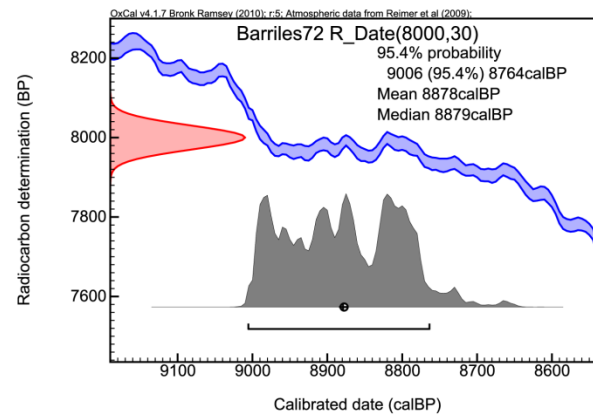
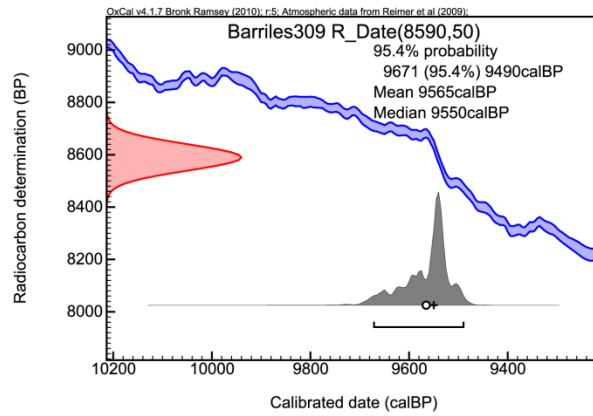
Ti Intrusives – coarse-grained gabbro in isolated areas of the Cordillera (*Stewart, 1978*). These units may include: granodiorites, quartz-diorite, diorite, and gabbro (*Ministry of Industry and Commerce, 1976*).

TK Cretaceous-to-Paleogene – Accreted volcanic seamounts and associated sedimentary units; dominates Panama’s interior western highlands. (*Buchs et al., 2009*)

Radiocarbon Plots

Barriles Deposit, Volcan Baru

Curve: IntCal 09



Caisan Deposit, Volcan Baru

Curve: IntCal 09

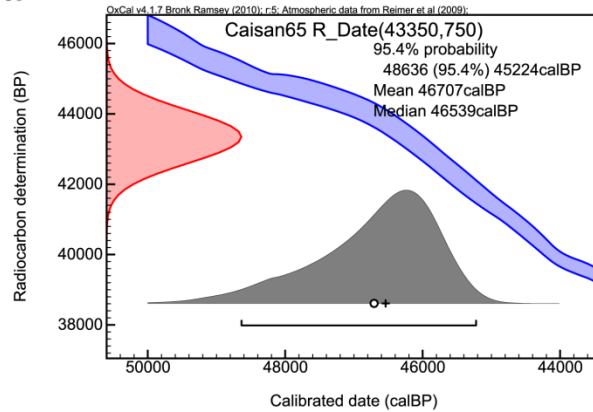


Figure 30 Radiocarbon Plots: Barriles and Caisán samples: 309, 072, and 065.

Map of Hummock Orientations

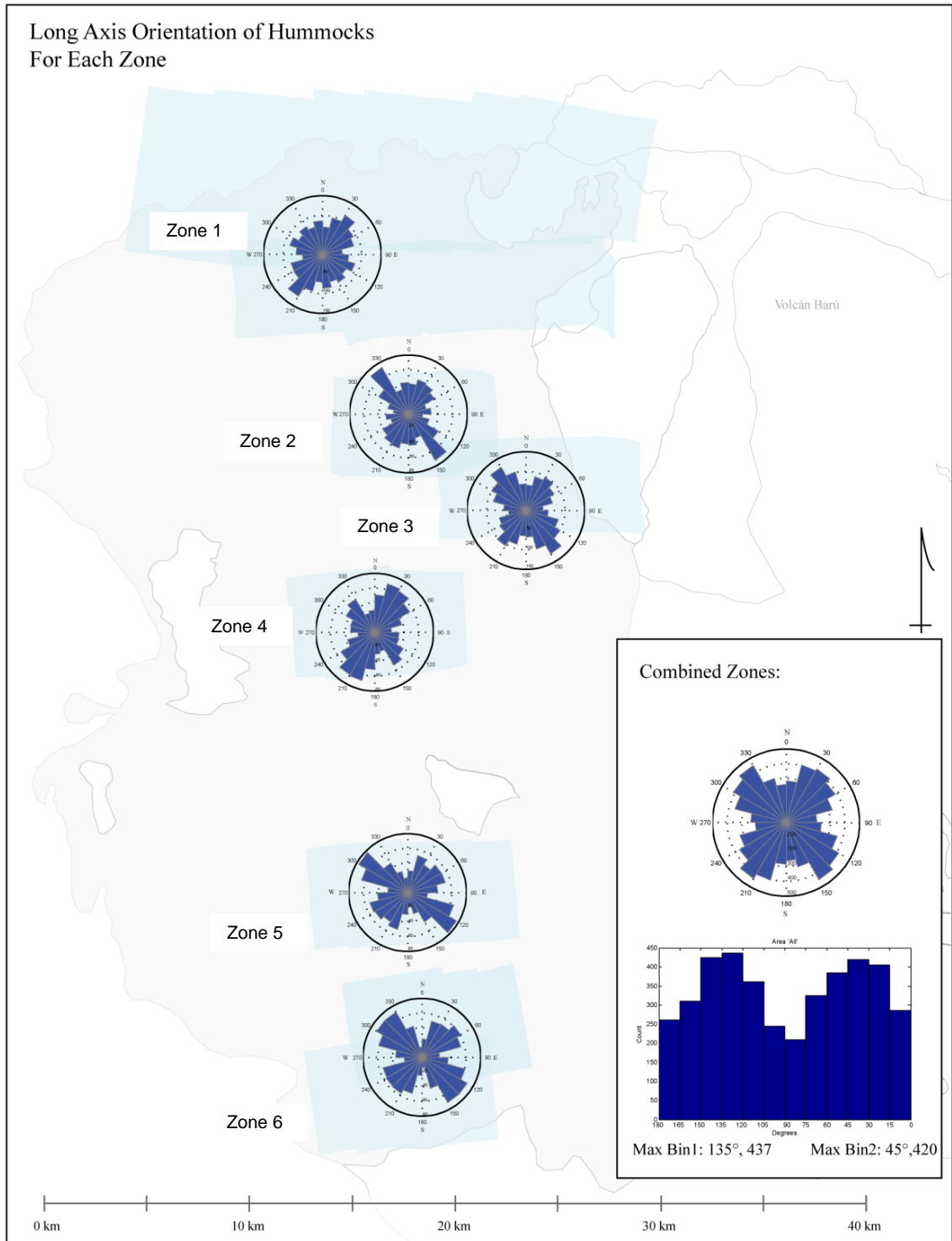


Figure 31 All 6 hummock zones were analyzed for orientations and summarized for the entire dataset.

Maps of Deposits and Hummocks

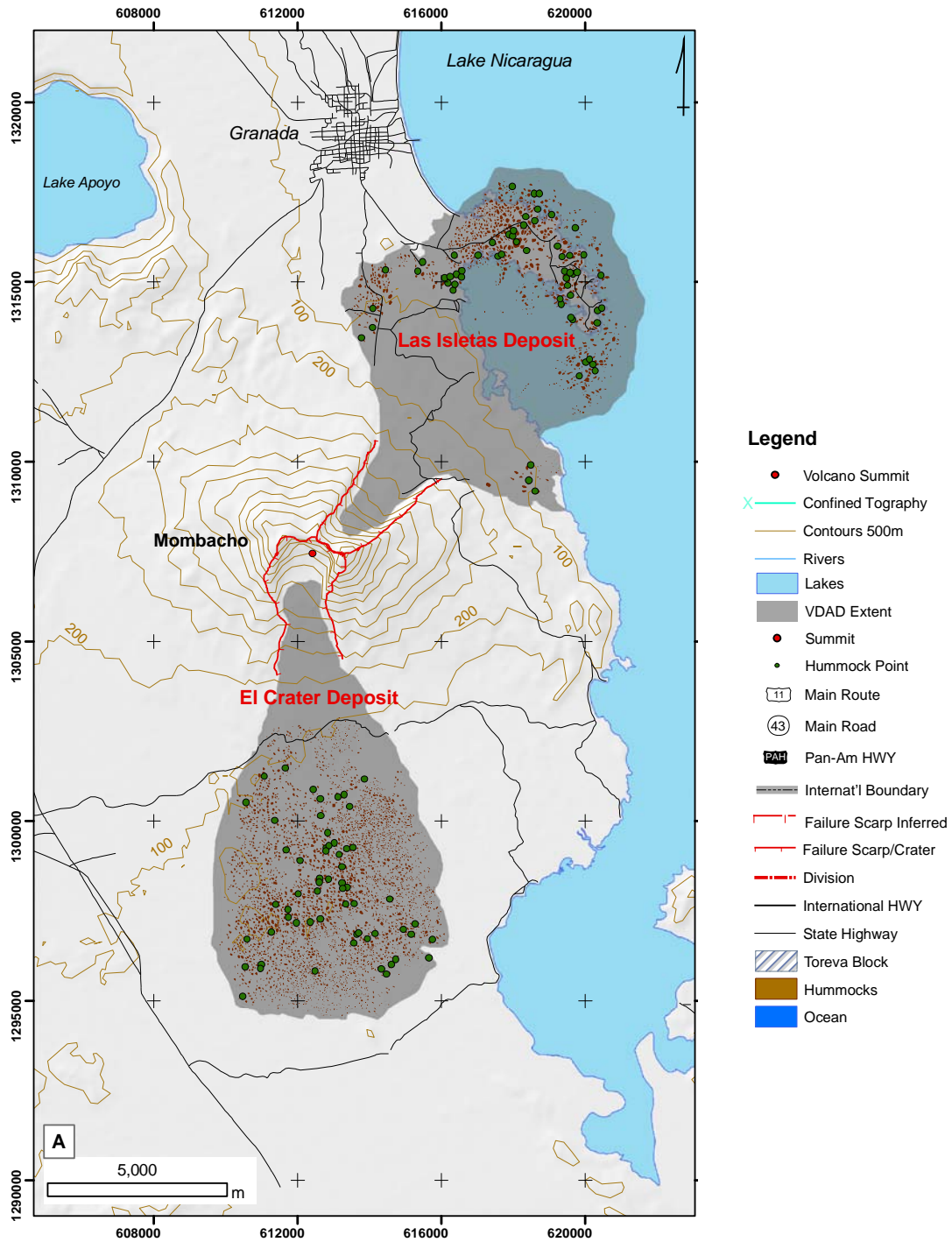
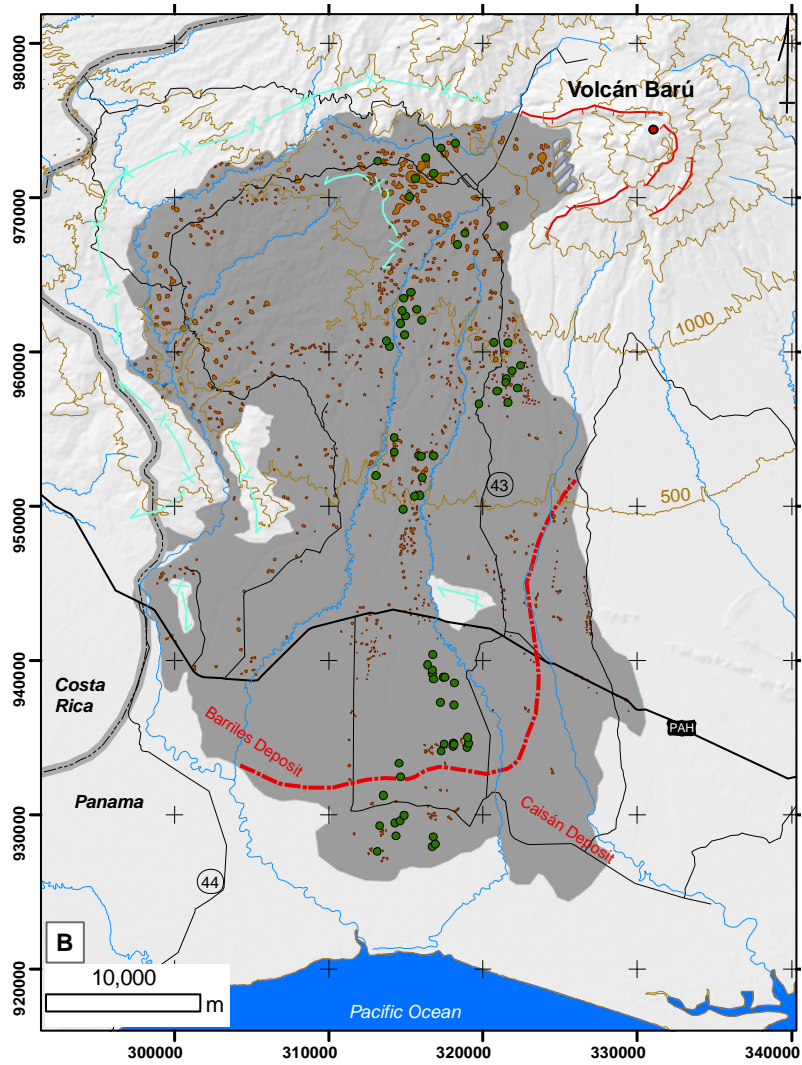
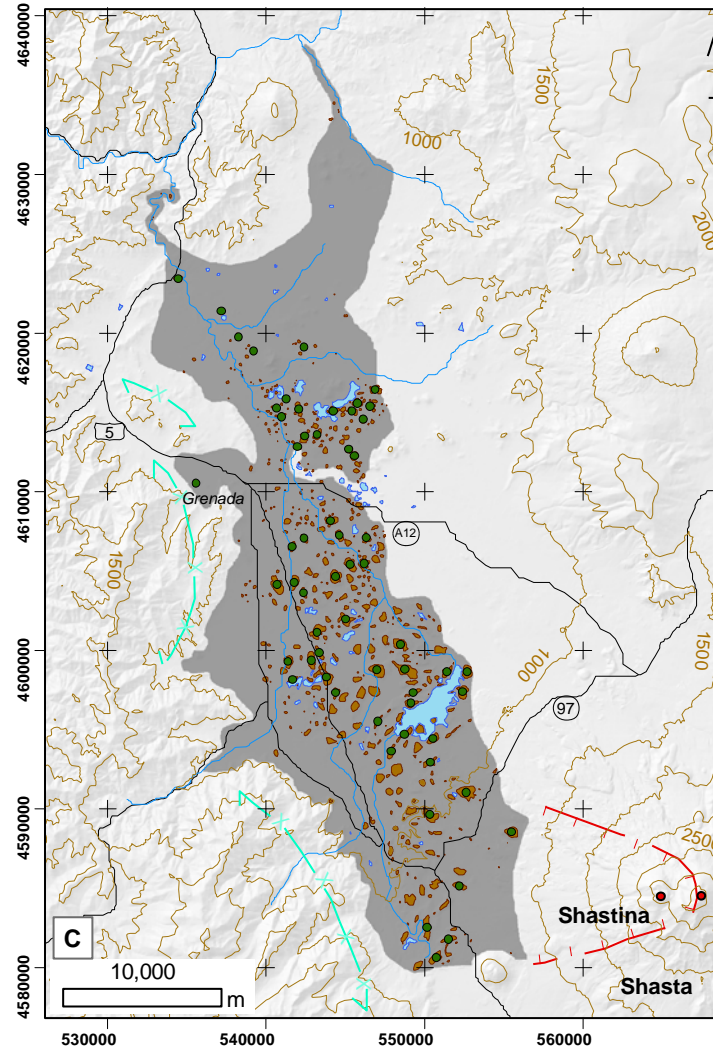


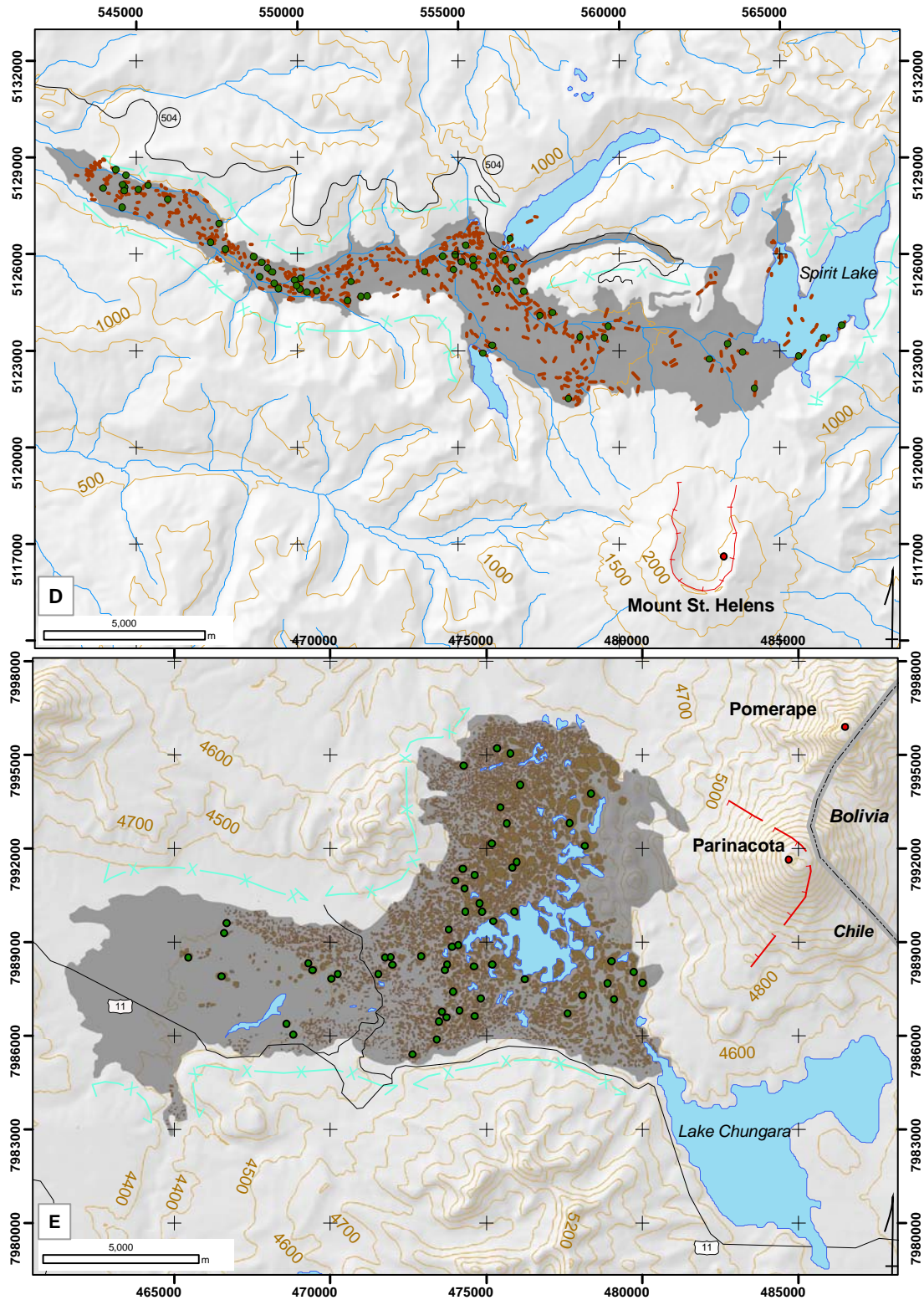
Figure 32 Six examples of VDADs from five volcanoes located in different countries. This page: A: Mombacho Volcano, Granada Department, Nicaragua (next 2 pages have locations B,C,D,E)



B: Volcán Barú, Chiriquí Province, Panama



C: Mount Shasta, California, USA



D: Mount St. Helens, Washington, USA
 E: Parinacota, Parinacota Province, Chile